1996

The effect of heterogeneous nucleation on two dimensional phase transformation kinetics

William Scott Tong
Lehigh University

Tong, William Scott

The Effect of Heterogeneous Nucleation on Two Dimensional Phase...

October 13, 1996

The Effect of Heterogeneous Nucleation on Two Dimensional Phase Transformation Kinetics

by

William Scott Tong

A Thesis

Presented to the Graduate and Research Committee

of Lehigh University

in Candidacy for the Degree of

Master of Science

in

Materials Science and Engineering

Lehigh University

August 1996

This thesis is accepted in partial fulfillment of the requirements for the degree of Master of Science.

8/22/96
(Date)

Thesis Advisor

Thesis Advisor

Department Chairperson

Acknowledgments

I wish to express my sincere gratitude to my advisors, Dr. Katy Barmak and Dr. Jeffrey Rickman for their supportive advice and tutelage, as well as precious time.

I would further like to thank Lehigh University and the National Science Foundation (Grants 9485000 and 9485023), for their financial support.

Finally I would like to thank my family, without whose support this thesis, as well as my mental health would not exist.

Contents

List of Figures

Abstract

In this thesis I examine quantitatively the effect of heterogeneous boundary nucleation on transformation kinetics. This is accomplished by using computer simulation and concurrent theoretical analyses to model the temporal evolution of microstructures resulting from catalyzed nucleation in an idealized two-dimensional system. Several quantities are calculated in order to probe the dynamics of phase formation. The spatial correlations among transforming regions are described by non-equilibrium correlation functions which summarize, for example, the area fraction of the system transformed at a given time and the size of small islands of untransformed material at late times. In addition, we undertake a detailed geometrical analysis of the terminal microstructures, analyzing the probability distribution of normalized grain areas and average perimeter, in order to identify the relevant length scales in the system. In general, a quantitative analysis of area fraction transformed and product microstructure reveals the existence of two length scales, one related to the internuclear separation and one related to the underlying cell size, whose ratio determines various regimes in the evolution process and dictates the morphology of the final microstructure. The benefit of this study is that it also provides an intuitive understanding of how important transformation parameters, such as the nucleation density and the underlying cell diameter, determine the course of the

transformation and its end result.

Overview

The necessity for understanding the kinetics of phase formation and its impact on microstructure is well known. In first-order phase transformations, for example, energetic considerations often dictate that nucleation occurs preferentially on crystal defects, such as grain boundaries, rather than homogeneously throughout the bulk material with the result that the microstructure of the evolving phase is spatially and temporally correlated, to some extent, with the distribution of these defects. In order to explore these important correlations in more detail we have undertaken here an investigation of the the effects of boundary nucleation on transformation kinetics and microstructure. This investigation consists of two complementary studies, the first involving the description of the spatial and temporal evolution of microstructure, and the second a detailed characterization of the geometry of the resulting "final" structure prior to grain growth. In both components of this work computer simulation is employed in order to model phase formation and growth, and this approach is then coupled with analytical calculations in order to more fully describe the features of the evolving phase.

In particular, the first study embodies an examination of the temporal evolution of a phase through simulation and analytical calculation of relevant n-point correlation functions. As the name implies, these functions can describe, for example, the

fraction of material transformed at a given time (the one-point function) and the approximate size of small domains of untransformed material at late times (higher n-point functions). The object of this work is to understand quantitatively how the spatial distribution of catalytic sites affects the character of the evolving phase. As will be seen below, it is possible to identify various temporal regimes during a given transformation, the length of each regime depending critically on the distribution of nucleation sites. One benefit of this analysis is that it also provides a n intuitive understanding of the relation between the geometry of the catalytic sites and that of the product grains.

Building on this intuitive understanding, the second study focuses on the correlation between nucleation site geometry and resultant product grain structure through analysis of the probability distributions of normalized product grain area and perimeter. As expected, the character of the area and perimeter distributions can be attributed to the relative values of two length scales in the system: the average internuclear spacing and the average cell length. The purpose of this work is to understand the relation between the important transformation parameters and the final microstructure. As will be seen, it is possible to identify three behavior regimes of the probability distributions resulting from different kinetic parameters, characterized by the length scale ratios. As a result of this analysis, a quantitative description of the role that nucleation site geometry plays on resultant microstructure has been developed.

The intuitive understanding between nucleation site position and resultant phase formation developed in this thesis introduces potential research that would be difficult without such knowledge. For example, this work exclusively examines nucleation occurring as a burst, when it is conceivable that nucleation could occur

constantly with time, or even as a more complex function of time. One would expect considerably different results than those from this work, since time-dependent nucleation embodies distinctly different nucleation conditions. Another interesting topic of study would be the addition of mechanisms, such as grain boundary coarsening, that would allow a more realistic structure to be simulated. Other avenues of research could include investigation of higher n-point correlation functions to further elucidate the role that catalytic nucleation has on resultant microstructure.

Chapter 1

Impact of Heterogeneous Boundary Nucleation On Transformation Kinetics and Microstructure

1.1 Introduction

The necessity for understanding the kinetics of phase formation and its impact on microstructure has provided the impetus for a number of experimental and theoretical studies in various fields. For example, the correlation of microstructural features with mechanical properties, such as ductility and yield strength, is well established in bulk eutectoid steels below the austenitic transformation temperature. Further, in the case of thin films, reactive phase formation of silicides [1] is used to obtain the desired electrical contact properties in microelectronic devices. More generally,

theoretical investigations of the decay of metastable states via nucleation and subsequent growth in a number of idealized model systems, including spin and phase-field models, have been instrumental in testing theories of homogeneous nucleation and have provided substantial insight into the mechanisms of late-time coarsening (i.e., Lifshitz-Slyozov) kinetics. [2, 3]

One general and rather useful description of the temporal evolution of a phase transformation, given by Kolmogorov [4] and later by Johnson, Mehl and Avrami [5] (hereafter referred to as JMA), involves the calculation of the fraction of reactant phase transformed in terms of the nucleation rate, possible grain growth mechanisms and effective spatial dimensionality. The inference of such rates and mechanisms from experimentally measured transformation fractions is somewhat problematic, however, as the parameters in the JMA equation do not uniquely define the kinetics of the system. A complete description of the time evolution of a phase transformation in some system would require a knowledge of the probability distribution of an appropriately defined phase field at all space-time points. As this distribution is generally not known, except in some very special cases, one tries to investigate spatial correlations in a transforming system by calculating a small number of nonequilibrium, equal-time, n-point correlation functions. Indeed, Sekimoto [6] has derived general expressions for these functions for idealized models of phase nucleation and growth. The JMA equation, for example, embodies the one-point correlation function and so does not yield any information on the size of the product phase as a function of time. More recently, Yu and Lai [7] have adopted a similar formalism and revisited a number of cases previously addressed by Cahn. [8]

The goal of the present paper is to describe the evolution of phase formation in a two-dimensional system in which nucleation is spatially biased to occur on the sites of

a network representing an underlying grain structure. The motivation for this work is to obtain a better understanding of the kinetics of reactive phase formation in thin films and, in particular, to elucidate the role of site-biased nucleation on subsequent growth and product phase morphology. There has been a great deal of experimental work in the general area of thin film reactions[9, 10, 11, 12, 13, 14, 15, 16, 17] given the technological implications, but the complexity of such reactions has dramatically slowed parallel theoretical efforts. In particular, little work has been done to establish an integrated theory of nucleation and growth in these systems and, in addition, the importance of heterogeneity in nucleation has not been considered. It should be pointed out here, however, that the foundation for the present study was established some years ago in pioneering work by Cahn [8] on the kinetics of grain-boundary nucleated reactions and its application, in a simplified form, to thin film reactions by Coffey et al. [14] Now, in this work, computer simulation is combined with the analytical calculation of non-equilibrium correlation functions in order to describe the temporal evolution of a two-dimensional transformation which is governed essentially by interface kinetics. By contrast with previous work in this area, we consider in explicit detail the effect of a *complex underlying structure*, which catalyzes heterogeneous nucleation, on *product phase microstructure* and the transformation kinetics with particular attention to non-trivial, *late-time impingement effects*. Further, we relate our findings to experimental calorimetric investigations of phase formation in thin films [18, 19, 20] and to recent models of this phenomena which are based on rate equations.

This paper is organized as follows. In Sec. II the theoretical formalism is discussed and applied to both homogeneous and heterogeneous nucleation. In Sec. III the computer simulation methodology is outlined. In Sec. IV the results of our

computer simulations are compared with the theoretical predictions made in Sec. II. Section V contains an interpretation of the results and some conclusions.

1.2 Theoretical Formalism

1.2.1 Basic Equations and Homogeneous Nucleation

Consider a two-dimensional system consisting of given phase(s) in which droplets of a new phase can nucleate and grow. As a specific example of this, one can envision an interface between two homogeneous phases at which a reaction occurs and a new product phase is formed. Such reactions are known to occur in Nb/Al thin films and have been studied extensively using differential scanning calorimetry. [14] In this case the focus will be on growth in the interface plane neglecting, for the moment, transverse growth. For concreteness, we will assume that nucleation occurs in a burst at some initial time and that this results in a collection of grains, each taken to be circular, that grow in a regime dominated by interface kinetics. The radial growth rate of these grain is G. These simplifying assumptions are inferred from observations of nucleation and growth made in the aforementioned Nb/Al thin films [14]. Thus, this hypothetical system will serve as a model of nucleation and growth in reactive phase formation.

Given this description and following the work of Sekimoto [6], it is advantageous to define a phase field, $u(\vec{r})$, where $\vec{r}$ is a two-dimensional position vector, such that $u(\vec{r})$ =0(1) if the region at $\vec{r}$ is transformed (untransformed). With this definition one can then know the detailed time evolution of the system by determining the probability distribution, $P[\vec{u}(\vec{r}), t]$, for the phase field. Now since it is difficult, if not impossible, to obtain this distribution analytically, it is advisable to determine its

important properties by the calculation of equal time, n-point correlation functions defined by the functional integral

$$C_n(\vec{r}_1, \vec{r}_2, ..., \vec{r}_n, t) = \langle \Pi_{i=1}^n u(\vec{r}_i, t) \rangle, \tag{1.1}$$

where the angle brackets denote an average over an ensemble of nucleation events. This correlation function is the probability that none of the points $\vec{r}_1, \vec{r}_2, ..., \vec{r}_n$ is included in the product phase at time t.

Sekimoto has shown that this correlation function for our system can be expressed as

$$C_n(\vec{r}_1, \vec{r}_2, ..., \vec{r}_n, t) = \exp\left[- \int d^2r' \int_0^\infty d\tau I(\vec{r}', \tau) (1 - \Pi_{i=1}^n D(\vec{r}_i; t_i : \vec{r}'; \tau)) \right], \tag{1.2}$$

where $I(\vec{r}', \tau)$ is the nucleation rate per unit area at position $\vec{r}'$ and time τ and where $D(\vec{r}_i; t_i : \vec{r}'; \tau) = 0(1)$ if the point at $\vec{r}$ is transformed (untransformed). Further, since the system is translationally invariant, it is expected that D will only depend on space as $\vec{r} - \vec{r}'$ and will be determined by the circular droplet shape. Given this expression it should be noted that the total area fraction transformed of a system with area A as a function of time, t, is given by

$$\phi_A(t) = 1 - \frac{1}{A} \int d^2r C_1(\vec{r}, t), \tag{1.3}$$

a result which embodies the JMA equation. Thus, $C_1(\vec{r}, t)$ can be interpreted as the probability that the element of material at $\vec{r}$ is *untransformed* at time t. The interpretation of the higher-order correlation functions can be given in an analogous manner.

As an illustration of the formalism outlined above, consider a burst just after the origin of time that creates nuclei at spatially random locations in the aforementioned two-dimensional system. The nucleation rate corresponding to this burst and

resulting in a planar density, n, of nucleation sites can be written as

$$I(\vec{r}', \tau) = n\delta(\tau+), \tag{1.4}$$

where $\tau+$ is some time just after the origin of time. Upon inserting the nucleation rate in Eq. (1.2) one finds that

$$C_1(t) = \exp(-n\pi G^2 t^2) = 1 - \phi_A(t), \tag{1.5}$$

which is independent of position (as expected). This is the JMA equation for the two-dimensional case considered here. The calculation of the corresponding two-point correlation function is summarized in the Appendix. We note here that the extent of spatial correlations in the transforming system can be obtained by evaluating the normalized correlation

$$\chi(|\vec{r}_1 - \vec{r}_2|, t) \equiv \frac{C_2(|\vec{r}_1 - \vec{r}_2|, t) - [C_1^2]}{[C_1^2]} = -1 + \exp(n\pi G^2 t^2 \gamma(s)), \tag{1.6}$$

where

$$\gamma(s) = \frac{2}{\pi}\left[sin^{-1}\sqrt{1-s^2} - s\sqrt{1-s^2}\right]\Theta(1-s),$$
$$s = |\vec{r}_1 - \vec{r}_2|/2Gt \tag{1.7}$$

and where Θ is the Heaviside step function.

As a corollary to the last result, one can also infer the size of domains of both reacted and unreacted material as a function of time and thereby estimate the time dependence of reacted grain size. For example, if one defines a characteristic time $t_c \equiv 1/\sqrt{n}G$, then by examining the time dependence of the ratio of the two-point function and the one-point function, $C_2(|\vec{r}_1 - \vec{r}_2|, t)/C_1$, one finds that the characteristic unreacted domain size $l(t) \sim (t/t_c)^{-1}$ at late times (i.e., $(t/t_c) >> 1$).

1.2.2 Heterogeneous Nucleation: Line

Having investigated homogeneous nucleation, we next consider heterogeneous nucleation on an infinite line. This line will serve as a "building block" for more complex grain structures to be assembled below. In this case it is supposed that nucleation occurs in a burst just after the origin of time and is restricted to an infinite line, coinciding with the y-axis, which exists in a two-dimensional system. For this scenario the nucleation rate can be written as

$$I(\vec{r}', \tau) = \tilde{n}\delta(x')\delta(\tau+), \tag{1.8}$$

where $\tilde{n}$ is the linear density of nucleation sites and $\tau+$ is, again, a time just after the origin of time. Upon substituting Eq. (1.8) into Eq. (1.2) it is found that the one-point function can be written as

$$C_1(x,t) = exp\left[-2\tilde{n}\sqrt{G^2t^2 - x^2}\Theta(Gt - |x|)\right], \tag{1.9}$$

the translational invariance of the system in the y-direction yielding a result which only depends on the distance (x) from the nucleation line. The incorporation of the Heaviside step function, $\Theta(Gt - |x|)$, in the previous equation expresses the fact that, beyond a distance Gt from the line, no material is transformed. It should be noted here that a similar result was derived by Cahn for the case of nucleation on a line with a constant nucleation rate [8].

Finally, it is of interest to determine the area fraction transformed in a finite-size system with dimensions $L \times L$. This can be accomplished by noting that the fraction of material *untransformed* after time t is given (approximately) by

$$\left[1 - \frac{2Gt}{L}\right] - \frac{1}{L}\int_{-Gt}^{Gt} dx exp\left[-2\tilde{n}\sqrt{G^2t^2 - x^2}\right], \tag{1.10}$$

where the terms in the first square brackets represent material at a distance greater that Gt from the line and the integral represents material within a distance Gt from the line which is still untransformed. Upon making the convenient substitution $x = Gtcos(\psi)$ and inserting the resulting expression into Eq. (1.3) one obtains

$$\phi_A(t) = \frac{2Gt}{L}\left[1 - \frac{1}{2}f(0,\pi)\right] \tag{1.11}$$

where

$$f(a,b) \equiv \int_a^b d\psi sin(\psi) exp\left[-2\tilde{n}Gtsin(\psi)\right]. \tag{1.12}$$

Now, while it is possible to carry out the integration in Eq. (1.12) and express the result in terms of a Bessel series, it is perhaps best at this point to consider two limiting cases. First, in the limit of short times ($\tilde{n}Gt << 1$) $\phi_A(t) \rightarrow \tilde{n}\pi(Gt)^2/L$, consistent with the expectation that, prior to impingement, transforming regions grow as independent circles which originate from nuclei having an effective area density of $\tilde{n}/L$. By contrast, at late times, it is expected that the transforming region propagates essentially as two linear fronts. This can be seen by noting that the integrand in Eq. (1.12) is a sharply peaked function of ψ at late times and so a saddle-point integration yields

$$\phi_A(t) \rightarrow \frac{2Gt}{L}\left[1 - \frac{e^{-1}}{2}\sqrt{\frac{\pi}{2}}\frac{1}{(\tilde{n}Gt)^2}\right], (\tilde{n}Gt >> 1), \tag{1.13}$$

consistent with the motion of two (nearly) linear fronts.

1.2.3 Heterogeneous Nucleation: Effect of Grain Size

Since nucleation often occurs on some underlying structure, we now examine quantitatively the role of the grain size of this structure in determining the evolution path for phase formation. It is advantageous to consider first a relatively simple structure

consisting of a periodic array of N rectangular cells, each of width $l = L/N$, which tile a $L \times L$ system. With a given cell one can associate two parallel lines of semi-circular grains growing inward towards the grain center. For the regime $2Gt/l < 1$ these lines are effectively independent and so the area fraction transformed can be obtained from a superposition of the results for a single line to yield

$$\phi_A(t) = 2\alpha \left[1 - \frac{1}{2} f(0,\pi)\right] \Theta(1-2\alpha) \tag{1.14}$$

where $\alpha = NGt/L$ and the function $f(0,\pi)$ is defined in Eq. (1.12).

In the late time regime where $0.5 < \alpha < 1$ the bookkeeping for impingement effects becomes more complex as the two parallel cell lines can now transform some material in the same region. In effect, the two nearly planar fronts originating from cell lines begin to interpenetrate near the center of a cell. Upon accounting for this interpenetration one finds that

$$\begin{aligned} \phi_A(t) = [1 - 2\alpha f(\psi_1, \pi/2) - (\alpha - 0.5)] \times \\ \left[\int_0^{\pi} d\psi \sin\psi \exp[-2\tilde{n}Lg_+/N] \exp[-2\tilde{n}Lg_-/N]\right] \times \\ \Theta(2\alpha - 1)\Theta(2 - 2\alpha), \end{aligned} \tag{1.15}$$

where

$$g_{\pm}(\psi) = \sqrt{(\alpha)^2 - [(\alpha - 0.5)cos(\psi) \pm 0.5]^2} \tag{1.16}$$

and where $\psi_1 = cos^{-1}(1/\alpha - 1)$. In practice this correction to ϕ_A due to interpenetration is only significant at relatively low linear nucleation densities as low densities lead to increased corrugation in the propagating fronts and, hence, less material transformed in a given time. Further implications of this equation will be discussed in the next section where a direct comparison is made with the results of computer simulation.

The impact of a more complex underlying structure on phase formation can be assessed by considering, for example, an array consisting of square cells, each of dimension $L/N \times L/N$. As in the case of the one-dimensional cell structure discussed above, the transformation of square cells can be viewed in terms of the motion of fronts emanating from boundaries. An additional complication exists here, however, as fronts originating from orthogonal sides partially interpenetrate at early times. Nevertheless, it is also possible to calculate $\phi_A(t)$, incorporating this new feature, with the result that

$$\phi_A(t) = \left[4\alpha\left(1 - \frac{1}{2}f(0,\pi)\right) + 4\alpha^2\left(-1 + f(0,\pi) - \frac{1}{4}f(0,\pi)^2\right)\right]\Theta(1-2\alpha). \quad (1.17)$$

In the regime $2\alpha > 1$ it is necessary to amend Eq. (1.17) to account for further impingement effects. In practice this is not an important correction, except at small, linear nucleation site densities, and hence we will ignore this small effect for the moment.

1.3 Simulation Methodology

In this Section we briefly describe the methodology employed to simulate phase formation in a two-dimensional system of area A subjected to periodic boundary conditions. As the details of this approach have been related elsewhere [21] and employed in other investigations [22] only a brief outline containing the essential ingredients will be given below.

In order to efficiently simulate phase formation it is useful at the outset to superimpose a discrete square grid over the two-dimensional system under consideration. As will be seen below, this construct greatly simplifies the bookkeeping operations

that must be performed to track the motion of the evolving phase at the price of limiting, to some extent, the spatial resolution that may be achieved. As will be evident from the results, this introduction of a short-wavelength cutoff is not particularly problematic.

The simulation begins with the nucleation of a given number of sites, all of which are introduced as a burst at one time, with a predetermined spatial distribution. In the case of homogeneous nucleation this distribution is spatially uniform, on average, and so there are no preferred sites. By contrast, in the case of heterogeneous nucleation, a particular underlying substructure is identified, and each site on the substructure acts as a potential nucleation site of the same strength. For simplicity, in this latter case it is assumed that all sites not on the given substructure are unavailable for nucleation. In this way the substructure, in effect, catalyzes nucleation.

After the determination of the nucleation site distribution, product grains originating from these nuclei are assumed to grow at a constant radial growth rate G. In particular, each element of a grain perimeter grows in this manner until it impinges on another grain. The transformation proceeds until all untransformed material has been exhausted. Thus, a space-time summary of the transformation involves cataloging, at each time, which positions have been transformed and noting the associated transforming grains. This is accomplished by first subdividing the grid into large squares and compiling a list of grains which are potentially responsible for transforming a particular square. This operation has the benefit of reducing the number of growing grains which must be monitored for a given region of the grid. Having obtained this list for each square, each gridpoint within a given square can be examined to determine which grain from the appropriate list first intercepts it and

the associated transformation time. The result of repeating this operation for each grid point is a table which summarizes the space-time history of the transformation, facilitating the calculation of the desired n-point correlation functions.

As it is essential to obtain good statistics for the computation of these correlation functions, the final results presented below represent averages over many realizations of the distribution of nucleation sites on a given substructure. Various substructures have been employed including: a one-dimensional lattice, a monodisperse square lattice, a polydisperse square lattice and a substructure generated from an independent nucleation and growth transformation. In the simulations we have systematically varied the site density and, in some cases, the system size in order to examine the impact of different length scales on our results. As we are particularly interested in correlating microstructure with kinetics, we also produce snapshots of the lattice which visually document the evolving transformation.

1.4 Results

In this Section the results of computer simulations are used to validate the theoretical description of phase formation that has been discussed previously and that will be augmented below. In particular, the kinetics of spatially random nucleation will be compared and contrasted with the kinetics associated with heterogeneous nucleation which is biased on the sites of an underlying network. For simplicity and in order to illustrate the basic features of the latter process, we consider "simple" geometric networks that permit a concurrent, tractable analytical study. In effect, we seek to understand the roles of two relevant length scales, the first set by the initial internuclear separation $(1/\sqrt{n})$ and the second set by the network

grain size (denoted by l). Finally, we explain how our results can be generalized to describe heterogeneous nucleation on more complex and, hence, more realistic grain structures.

The time evolution of a transformation, corresponding to one realization of spatially random nucleation and subsequent growth on a 240 x 240 square lattice, is summarized pictorially in Fig. 1.1. It is assumed that grains grow as circular disks prior to impingement, and that the growth kinetics is interface-controlled. Clearly, there is an initial time regime, set essentially by $1/\sqrt{n}G$, in which the disks grow independently followed by a regime in which impingements alter the evolving structure. It is worth noting here that these computer generated microstructure do indeed bear a close resemblance to what is actually seen in, for example, *in situ* transmission electron microscope images of crystallization of amorphous $CoSi_2$. [23] Figure 1.2 shows the area fraction transformed, ϕ_A, as a function of $n^{1/2}Gt$, for a series of transformations, each having a different initial nucleation site density, as determined from simulation.

As is evident from the figure, this series of transformations can be described by a universal curve, as expected from Eq. (1.5). As a further check on the consistency of the simulation results, the product phase growth rate, G and the areal nucleation site density, n, have been extracted for each case and shown to be in excellent agreement with the corresponding input values. Further, we have calculated the logarithm of the normalized two-point correlation from simulation and compared it with the expected result (Eq. (1.6)) in Fig. 1.3, thereby confirming the form of the universal function $\gamma(|\vec{r}_1 - \vec{r}_2|/2Gt)$ which describes the spatial decay of correlations among transformed regions at $\vec{r}_1$ and $\vec{r}_2$.

Having characterized phase formation following homogeneous nucleation, we now

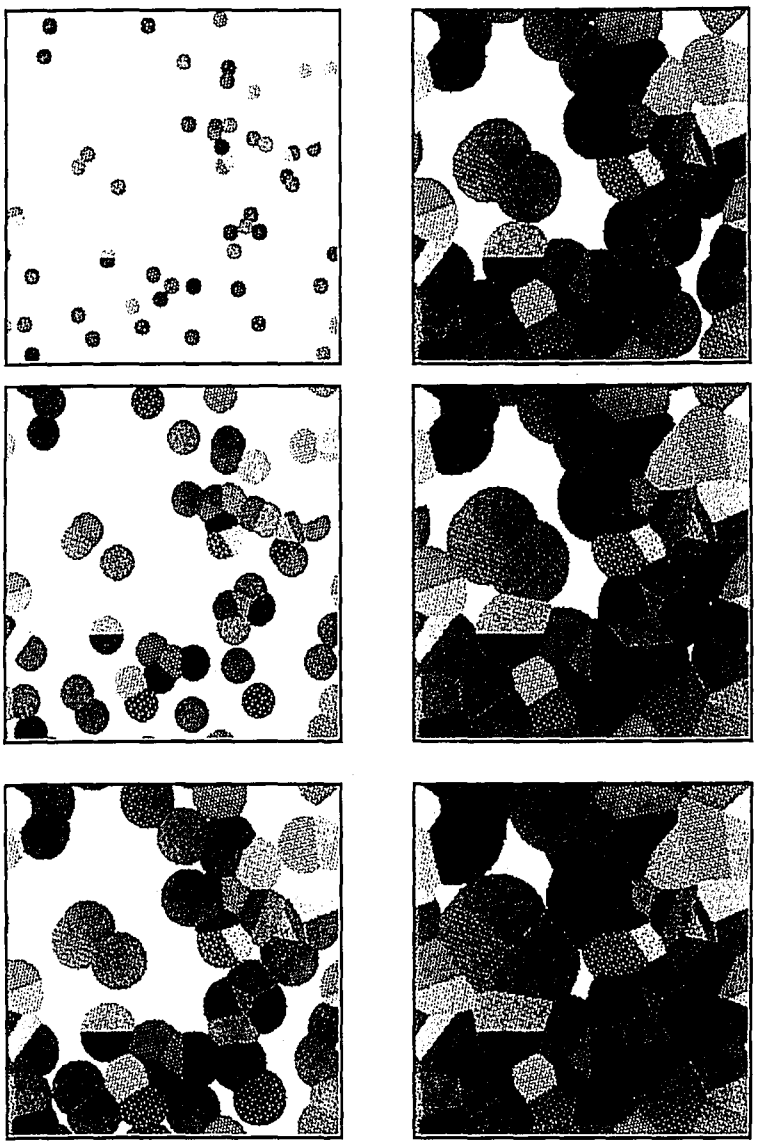

Figure 1.1: The time evolution of a transformation on a 240 x 240 square lattice (with periodic boundary conditions) which begins with a burst of nuclei at spatially random positions and is followed by the growth of circular droplets. For this case the areal nucleation density n = 9.89 x 10^{-4}, in units of a^{-2} (where a is the unit lattice parameter), and the snapshots correspond to reduced times $n^{1/2}Gt$ = a.) 0.22, b.) 0.41, c.) 0.63 , d.) 0.69, e.) 0.94 and f.) 1.13.

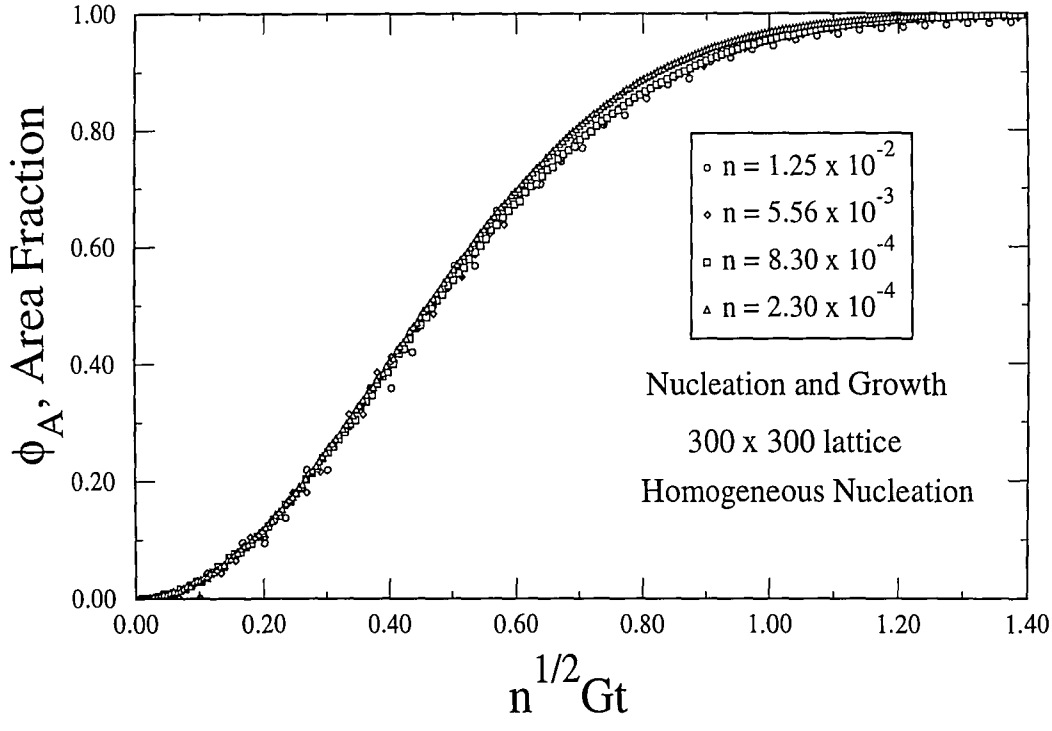

Figure 1.2: The area fraction transformed, ϕ_A, as a function of $n^{1/2}Gt$, for a series of transformations, each having a different initial nucleation site density, as determined from simulation. It should be noted that the data collapse onto a universal curve, as expected. These results represent averages over approximately 60 independent initial configurations for each density.

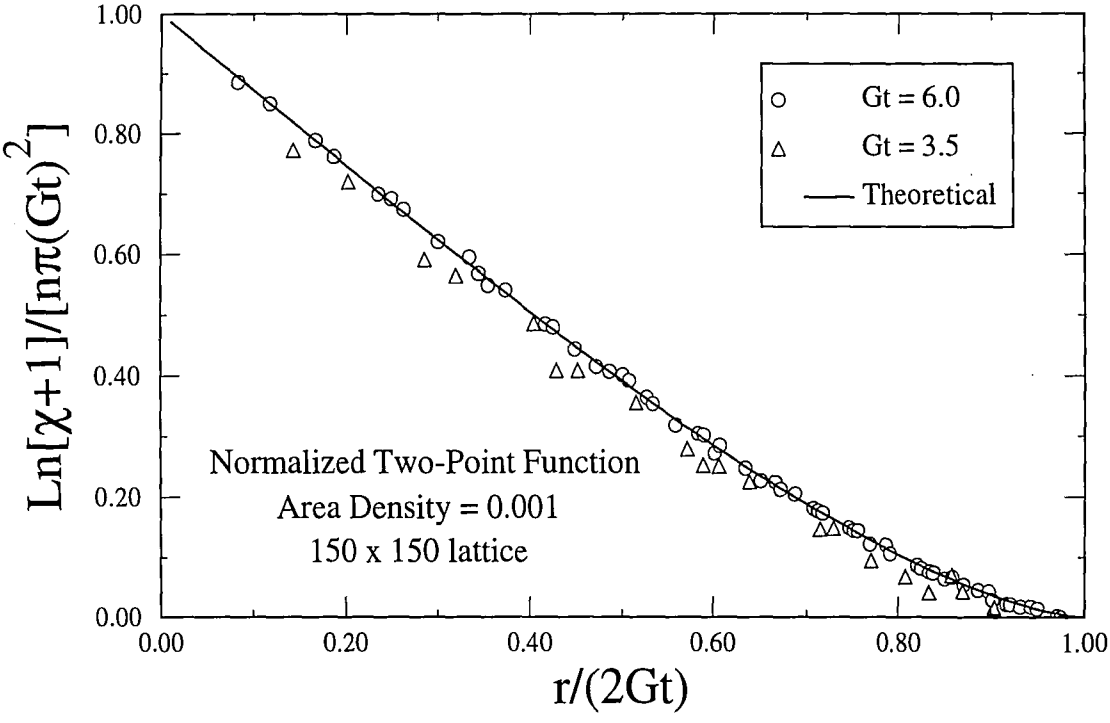

Figure 1.3: The logarithm of the normalized two-point correlation, as determined from simulation, compared with that predicted by Eq. (1.6) for two different areal nucleation densities n. The simulation results were obtained for a 240 x 240 square lattice. This confirms the form of the universal function $\gamma(|\vec{r}_1 - \vec{r}_2|/2Gt)$ which describes the spatial decay of correlations among transformed regions. These results represent over 100 averages over initial configurations.

review simulations in which nucleation occurs preferentially on an underlying structure. Paralleling the theoretical development in the previous section, we first consider a pseudo-one-dimensional structure consisting of an array of parallel lines. For concreteness, it is assumed that a 240 x 240 square lattice is divided into rectangular cells with dimensions 120 x 240. Nucleation is taken to occur only on cell boundaries, and the probability of nucleation on any boundary is independent of position. Thus, an additional length scale, namely the cell size, has been introduced into the problem. It is expected, then, that fronts emanating from the cell boundaries will meet at the center of a cell, though some material will remain untransformed owing to the corrugation of these boundaries. This effect is shown convincingly in Fig. 1.4 and is, in fact, embodied in Eq. (1.13).

The results of a number of simulations with different linear nucleation densities are given in Fig. 1.5 which shows ϕ_A as a function of the reduced time, NGt/L.

Also shown in the figure are the analytical predictions for these curves, as obtained from Eq.'s (1.14) and (1.15). The agreement between the analytical predictions and simulation data is seen to be excellent, thereby validating the approach taken in the previous section.

Generalizing this cell model, we next consider a structure consisting of square grains of dimensions 100 $\times$ 100 which tile a 300 $\times$ 300 lattice, and nucleation is again taken to occur only on cell boundaries. As discussed earlier, in this case impingement effects are, not surprisingly, somewhat more complex than in the simpler, one-dimensional structure. Nevertheless, the analytical prediction of ϕ_A given in Eq. (1.17) faithfully describes the fraction transformed in the simulation, as shown in Fig. 1.6.

The influence of the under lying cell structure on product phase nucleation and

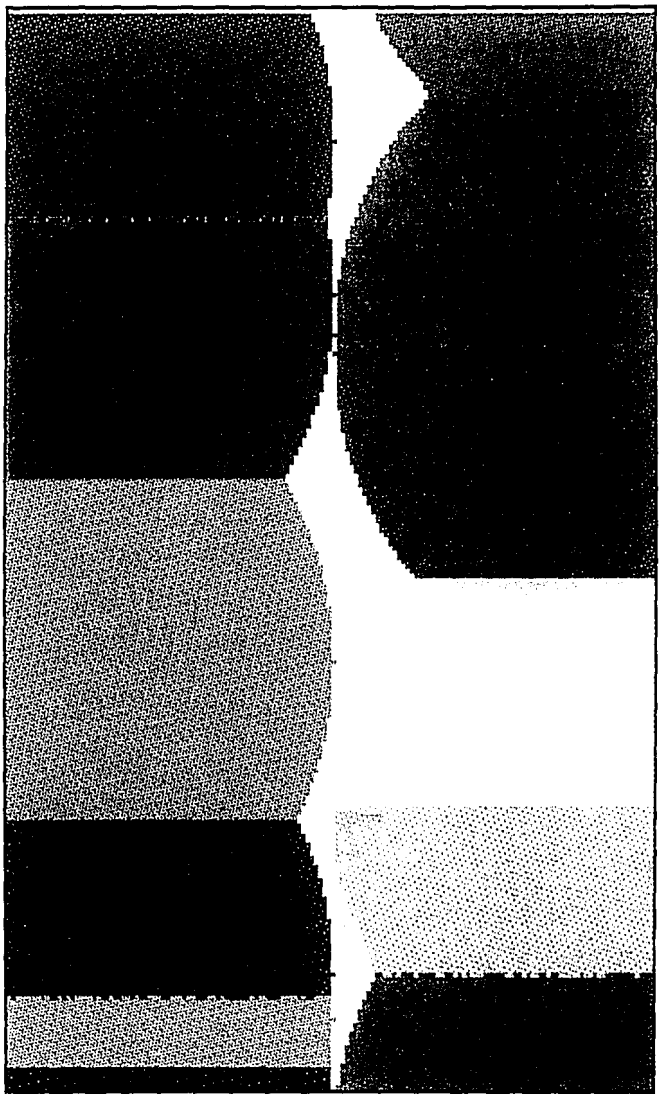

Figure 1.4: The meeting of two corrugated fronts emanating from cell boundaries at the center of the cell at $NGt/L = 1/2$. The corrugation evident in this figure results in some material remaining untransformed at this time.

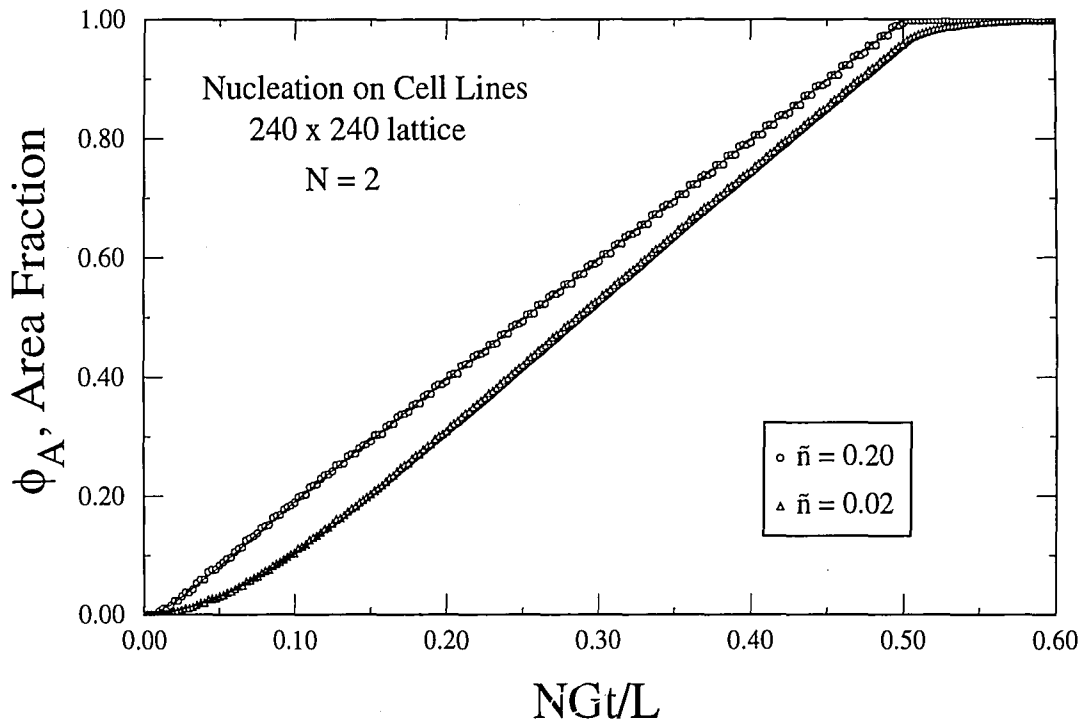

Figure 1.5: The area fraction transformed, ϕ_A, as a function of the reduced time, Gt/L for a pseudo-one-dimensional structure consisting of rectangular cells with dimensions L/2 x L which partition a L x L square lattice. In this case L = 240. Also shown in the figure are the analytical predictions for these curves, as obtained from Eq.'s (14) and (15). The agreement between the analytical predictions and simulation data is seen to be excellent. The results were averaged over 90 independent initial conditions.

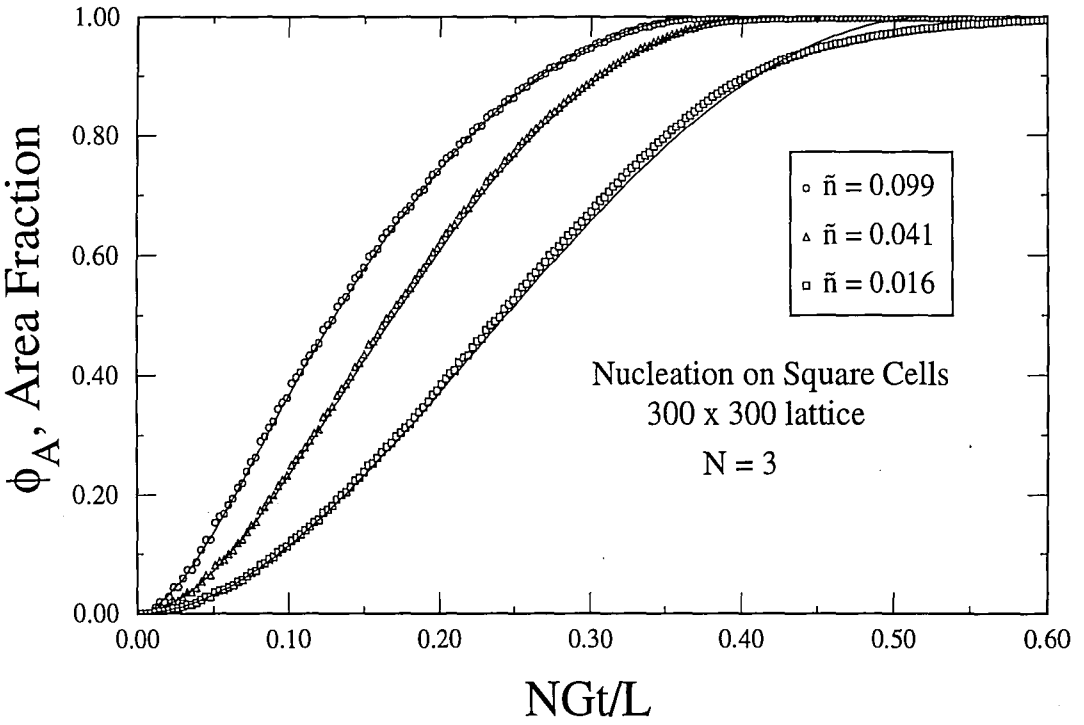

Figure 1.6: The area fraction transformed, ϕ_A, as a function of the reduced time, Gt/L, for a structure consisting of square grains of dimensions L/3 x L/3 which tile a L x L lattice. In this case $L = 300$. Again the simulation results are compared with the analytical prediction, Eq. (1.17), and the agreement is excellent. The results were averaged over 90 independent initial conditions.

growth can be seen by examining Fig. 1.7 which shows a time sequence of the transformation.

As is evident from the figure the underlying cell structure leads to elongated product grains with nearly parallel boundaries which mimic the symmetry of the underlying structure. Further, it is expected from stereology that along the boundary the product grain width is set by the internuclear spacing while, normal to the boundary, the product grain height is set by the underlying cell size.

As a further generalization of these results, we next consider a bimodal distribution of cell sizes, as modeled by two sets of squares having dimensions $l_1 \times l_1$ (75 x 75) and $l_2 \times l_2$ (150 x 150), respectively. The number of small (large) squares is M_1 (M_2). For relatively large linear nucleation site densities it is reasonable to approximate the area fraction transformed by a rule of mixtures wherein the large and the small squares transform independently. Clearly this approximation breaks down when product grains originating in one set of squares impinge on another set. This will most likely occur for low linear site densities and for large disparities in cell size. In order to test this hypothesis we simulated the aforementioned system and compared the results with those expected by an analytical rule of mixtures. Specifically, the rule of mixtures from this distribution is given by

$$\phi_A(t) \approx \frac{M_1 l_1^2 \phi_{A_1}(t)\Theta(l_1/2 - Gt) + M_1 l_1^2 \phi_{A_1}(t = l_1/2G)\Theta(Gt - l_1/2) + M_2 l_2^2 \phi_{A_2}(t)}{M_1 l_1^2 + M_2 l_2^2}, \tag{1.18}$$

where $A_1(A_2)$ is $l_1 \times l_1(l_2 \times l_2)$ and $\phi_{A1}(t)(\phi_{A2}(t))$ is the fraction transformed in the smaller (larger) squares. Figure 1.8 shows the area fraction transformed for this distribution of squares as determined directly from simulation and as predicted by Eq. (1.18) for a linear density $\tilde{n} = 0.20$.

The agreement between these two calculations is seen to be very good indeed.

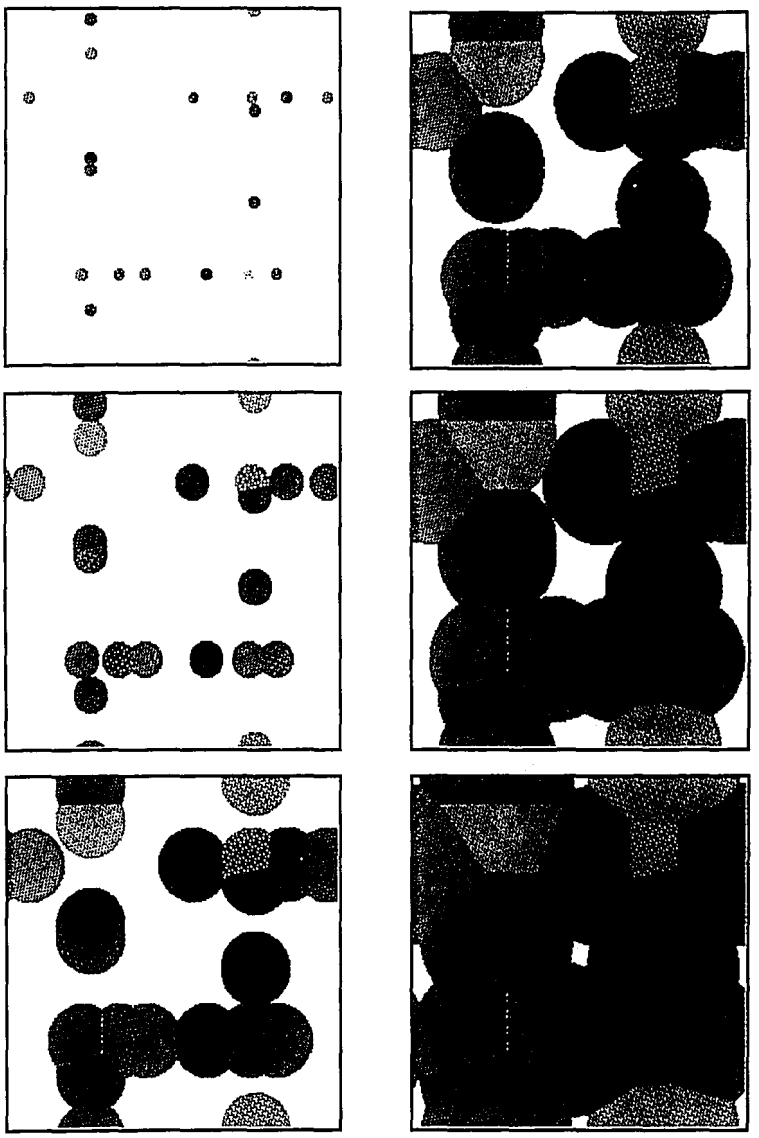

Figure 1.7: The time evolution of a transformation in which nucleation has occurred on the boundaries of square cells. In this series of pictures time increases from top to bottom and left to right. It should be noted that the underlying structure leads to elongated product grains with nearly parallel grain boundaries.

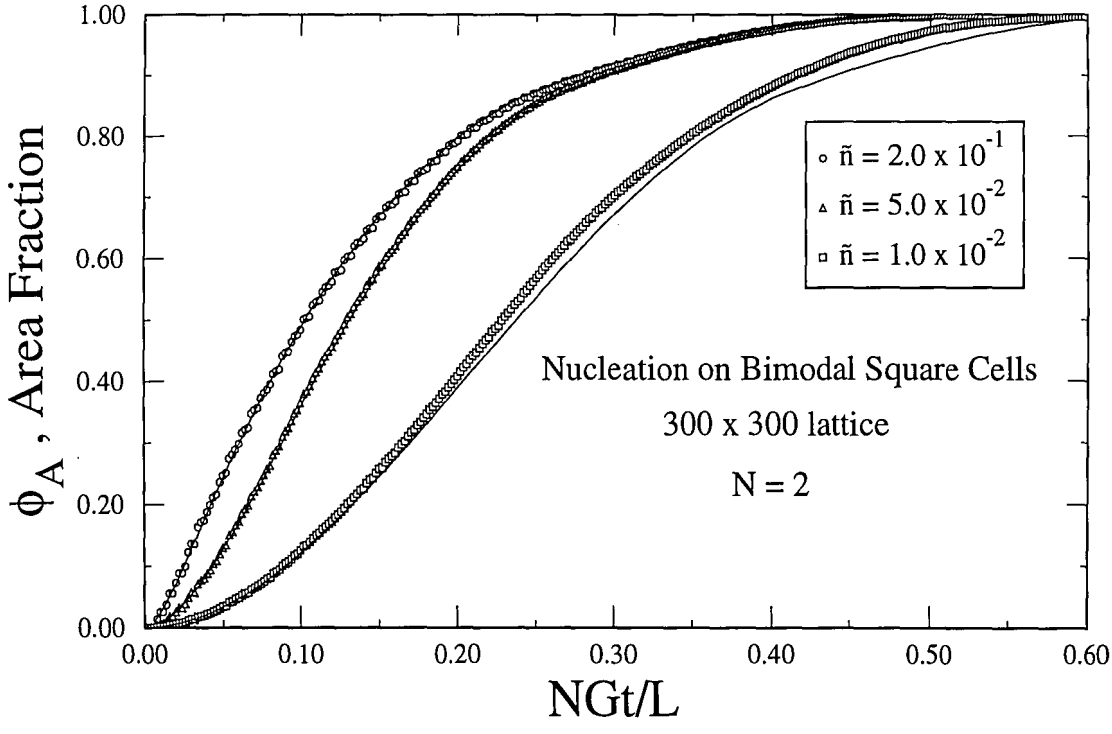

Figure 1.8: The area fraction transformed, ϕ_A, for a bimodal distribution of cell sizes, as modeled by two sets of squares having dimensions $l_1 \times l_1$ (75 x 75) and $l_2 \times l_2$ (150 x 150), respectively. The linear nucleation density here is $\tilde{n} = 0.20$. The simulation results are compared with an approximate rule of mixtures calculation, Eq.(1.18). The results were averaged over from 60 to 100 independent configurations.

Finally, it is of interest to examine nucleation on a more complex network of cells and subsequent growth in order to identify the general features of the transformation. With this in mind, an underlying structure was created from an independent microstructure generated by spatially random nucleation and growth. The sites on the boundaries of this structure served as preferential nucleation sites for the product phase. The resulting product phase distribution is shown in Fig. 1.9, clearly underlining the impact of the underlying structure on the transformation, and the time dependence of the associated area fraction transformed, $\phi_A(t)$ is presented in Fig. 1.10. The product phase microstructure shown in Fig. 1.9 demonstrates that the underlying structure leads to a number of parallel boundaries and non-equiaxed grains. The aspect ratio of these grains is still set, to a great extent, by the two inherent length scales as embodied in the internuclear separation and the underlying grain size. Now, an analytical description of of ϕ_A would require a more sophisticated rule of mixtures than employed above or, equivalently, an averaging of individual transformation fractions over the cell-size distribution. This is the subject of ongoing investigations.

1.5 Discussion and Conclusions

In this work we have used the theoretical formalism of Sekimoto [6] in parallel with computer simulations to investigate phase transformations in a two-dimensional system in which nucleation can be biased to occur on certain sites. The growth rate has been assumed to be constant in time so that the growing regions are circular in shape. The advantage of this formalism over that of the Johnson, Mehl and Avrami (JMA) is that the n-point correlation functions of Sekimoto, for $n > 1$, give

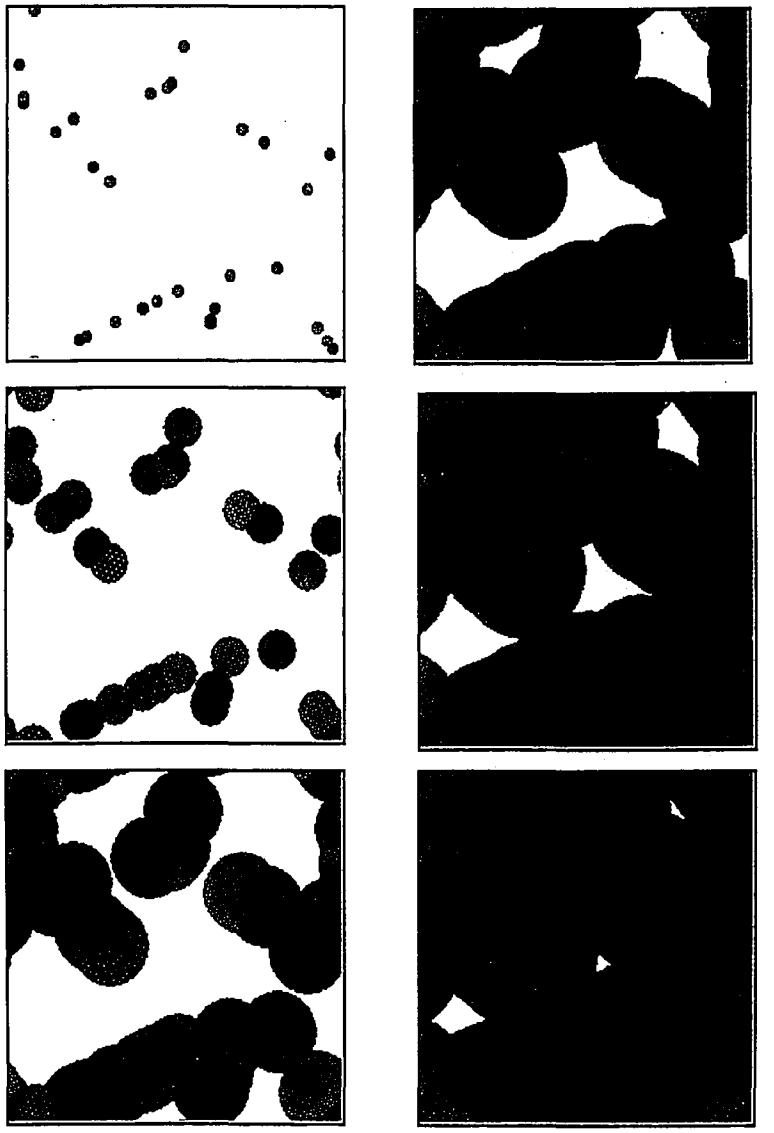

Figure 1.9: The time evolution of a transformation where nucleation occurs on a complex, underlying structure on a 240×240 lattice and the linear density of nucleation sites is $\tilde{n} = 0.035$. In this series of pictures time increases from top to bottom, and left to right. Clearly the underlying structure affects the microstructure of the product phase.

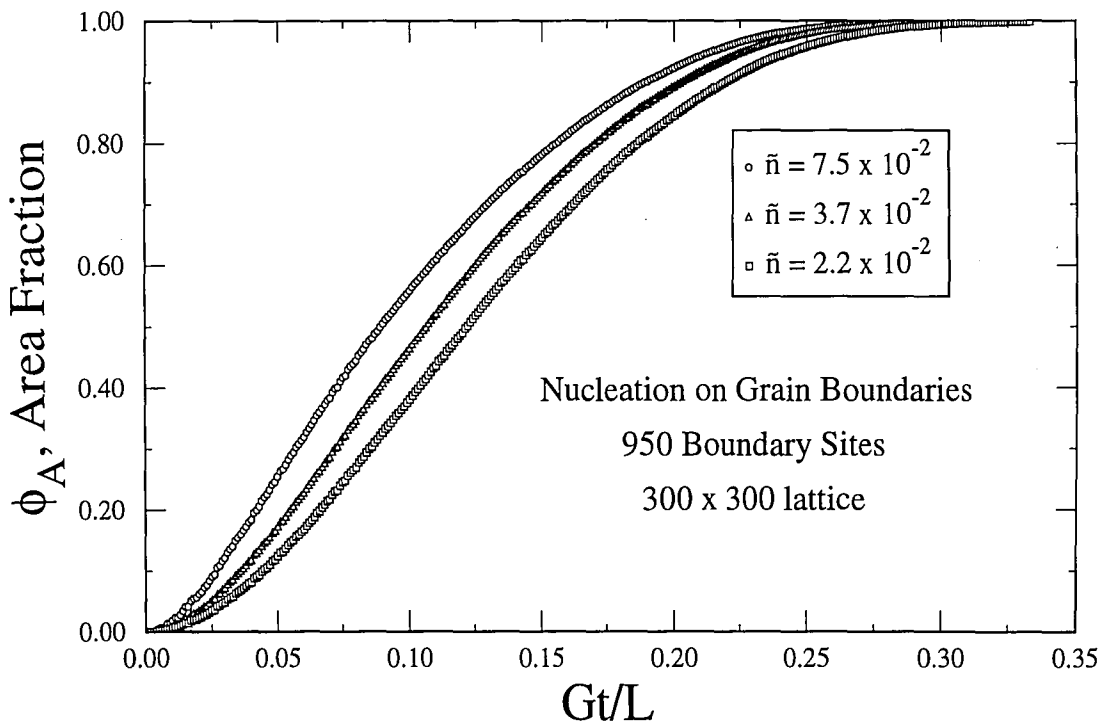

Figure 1.10: The time dependence of the area fraction transformed, $\phi_A(t)$, for the case described by Fig. 1.9.

information about the size of the (un)transformed regions. The JMA formalism embodies only the one-point correlation function and thus provides information only on the fraction (un)transformed.

Having investigated homogeneous nucleation, we then considered increasingly complex cases of site-biased nucleation. For a number of cases, we simulated an underlying structure starting with a single, infinite line and progressed to a one-dimensional cellular array, a monosized square array and finally a polydisperse array. These "simple" geometric networks were chosen because they permitted concurrent analytical investigations. In all cases, detailed impingement effects were incorporated in the analyses with the conclusion that the agreement between simulations and corresponding analytical calculations was excellent. Further, we have noted any limitations on the applicability of our method. Thus, we believe that the results of the present study significantly enhance our understanding of the kinetics of site-biased nucleation.

In addition, as mentioned in the Introduction, another motivation for the present work was to obtain a better understanding of the kinetics of reactive phase formation in thin films. A significant step towards this understanding was taken by Coffey et al., who provided an explanation for the unusual calorimetric traces for $NbAl_3$ formation in Nb/Al multilayers. [14] For this explanation Coffey et al. used Cahn's approach to nucleation and growth on a planar boundary. It was assumed that *homogeneous* product phase nucleation occurred in the Nb/Al interface as a burst and that the resultant grains grew at a constant rate and had circular traces in the interface plane.

It is important to explore the implications of the assumptions inherent in this homogeneous nucleation model for the Avrami exponent. It is expected that the

Avrami exponent in this case would be 2, independent of the multilayer periodicity. However, in recent calorimetric studies of Ni/Al [18], Ti/Al [19] and Nb/Al [20] multilayers, the effective Avrami exponent for the formation of the product phase has been found to vary as a function of multilayer periodicity, with values near 1 being frequently observed. These lower effective exponents manifest themselves as isothermal differential scanning calorimetry traces (i.e., power vs. time plots) that are broader than those associated with an exponent of 2. Given that the reactant phases in these multilayers are polycrystalline, we believe that our present work on site-biased nucleation provides a possible explanation for the observed anomalies. As evidence of this we show in Fig. 1.11 the time derivatives, $d\phi_A/dt$, obtained from simulation which would effectively determine the shape of the calorimetry traces.

It can be seen from the figure that the shape of the peak depends on the degree of heterogeneity of the nucleation process. Further work in this area currently focuses on direct microscopic observations of the evolving microstructure.

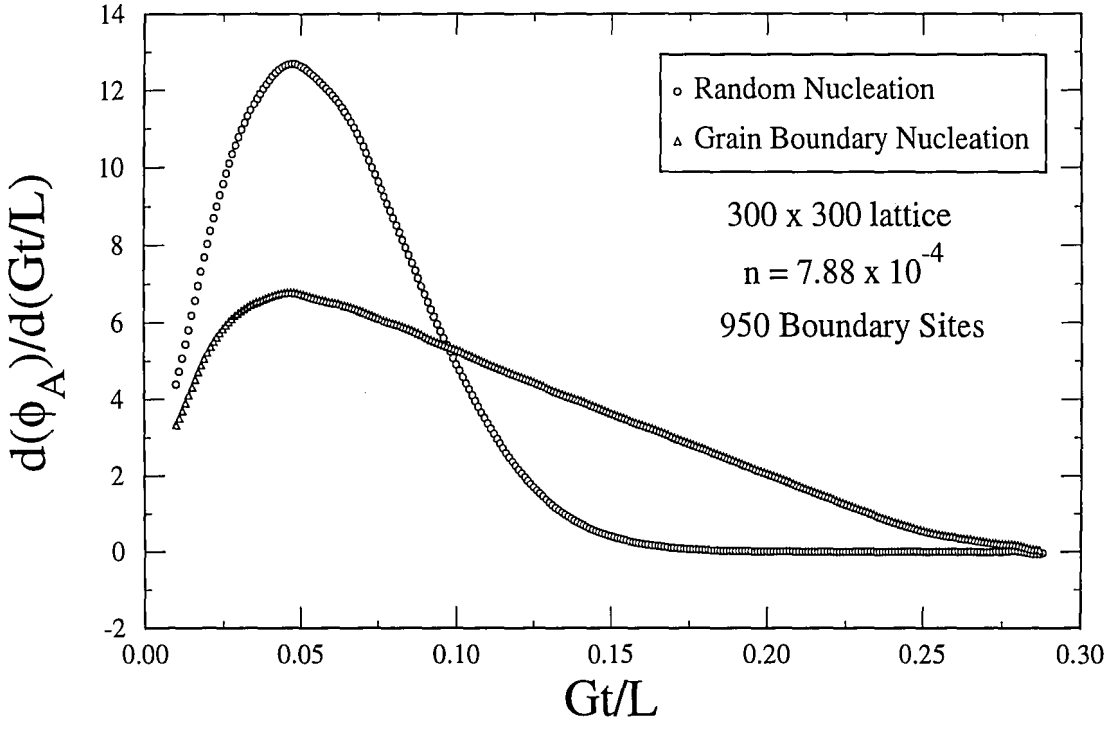

Figure 1.11: The time derivative of the area fraction transformed for cases of both homogeneous and heterogeneous nucleation. Clearly the width of the peak depends on the nature of the nucleation process.

Chapter 2

Impact of Heterogeneous Boundary Nucleation On Product Grain Size Distribution

2.1 Introduction

An analysis of the product microstructure resulting from a phase transformation can yield information on both the transformation kinetics and the distribution of any catalytic sites. For example, the grain structure of a metal solidified in a mold is critically dependent on the mold wall temperature and the presence of impurities which promote heterogeneous nucleation. Further, in many systems it has been found that the time dependence of the homogeneous nucleation rate correlates with rather sharp, straight phase boundaries separating Voronoi polygons in the case of a burst of nuclei at some initial time (the so-called cell model), while a more rounded phase morphology is associated with a constant nucleation rate (the Johnson-Mehl model)

[24]. More recently, a study of the kinetics and product microstructure resulting from boundary nucleated reactions suggested that, under some conditions, product grains are nonequiaxed due to the detailed shape of underlying grain boundaries [25].

While a number of metrics exist for the characterization of a given product microstructure, an analytic expression for the probability distribution of grain areas is generally not known, even for many idealized cases. In the aforementioned cell model, for example, an exact analytical description of the distribution of areas of generated Voronoi polyhedra is still lacking, although it has been possible to obtain the exact distribution variance [24] and an approximate functional form for the distribution [26]. Given the difficulty of completely characterizing microstructures resulting from homogeneous transformations, it is expected that a similar analysis of microstructures resulting from heterogeneous boundary nucleation will be problematic. Nevertheless, it is reasonable to assume that the locations of underlying catalytic sites will effectively determine both the sizes and shapes of product grains and that it should therefore be possible to extract some information about nucleation and growth mechanisms from a detailed geometrical analysis of these grains.

With this in mind, our goal in the present paper is to relate the morphology of a product phase created during a first-order transformation to the type and spatial distribution of preferred nucleation sites. This will be accomplished by a computer simulation study of phase formation in a model system. The motivation for this work is to obtain a better understanding of the kinetics of phase formation in thin films via a microstructural analysis. For concreteness and simplicity we consider a two-dimensional system of one phase which contains a known density of nuclei at some initial time. At subsequent times product grains of a second phase, originating

from this burst of nuclei, grow isotropically at a constant rate until impingement with other grains and, in so doing, consume the initial phase. It is further assumed that the grain growth kinetics is interface controlled and that nucleation can occur, in some cases, preferentially on a collection of sites to be specified. This simplified model of nucleation and growth captures many of the essential features of the early stages of reactive phase formation in metallic thin films and should provide some insight into the kinetics of such systems.

This paper is organized as follows. In Sec. II we briefly review the simulation methodology and describe the distributions of heterogeneous nucleation sites that are employed. In Sec. III histograms of grain area frequencies are analyzed in order to relate microstructural length scales to those of any underlying structure. This involves the calculation of moments of the grain size distribution and a determination of relevant control parameters. We also obtain finite-size corrections to our results from scaling arguments. Section IV contains a short discussion and some conclusions.

2.2 Simulation Methodology

In this section we briefly describe the methodology employed to simulate phase formation in a two-dimensional system subjected to periodic boundary conditions. While there are a number of useful schemes which can be used to describe phase formation, we have adopted here an established algorithm in which a discrete square grid is superimposed on the system of interest. The use of this grid greatly simplifies necessary bookkeeping operations that must be performed to track the motion of the evolving phases at the price of limiting, to some extent, the spatial resolution

that may be achieved. As the details of this approach can be found elsewhere [21] and have been employed in other investigations [25][22], only a concise outline will be given here.

The procedure begins with the random selection of nucleation sites from a given set of potential sites. For simplicity, these nuclei are introduced as a burst at one (initial) time. The set of potential sites is determined by the nucleation conditions that one wishes to describe. In the case of homogeneous nucleation the spatial distribution of nuclei is, on average, uniform and so there are no preferred sites. Thus, each lattice site is selected with the same probability. By contrast, in the case of heterogeneous nucleation, a particular underlying structure is identified, and each site on the substructure acts as a potential nucleation site of the same strength. In this latter case, it is assumed that sites not on the substructure are unavailable for nucleation, and so the substructure functions here as a catalyst. The underlying substructures employed here consist of a collection of Voronoi cells which fill the two-dimensional system. The average size of these underlying cells, denoted by l_u, is a tunable parameter which will determine, to some degree, the morphology of the resulting product microstructure.

Once the nucleation sites have been chosen, product grains originating at these nuclei are assumed to grow at a constant radial growth rate G, thereby simulating interface-controlled kinetics . Each element of a grain perimeter grows in this manner until it impinges on another grain, and the transformation proceeds until all untransformed material is exhausted. Upon completion of this process each grid point has been transformed by the growth front emanating from the nearest nucleation site. The grain area distribution of the final microstructure is simply determined by counting the number of lattice points that belong to each grain, taking

each lattice point to be a unit area. As it is essential to obtain good statistics for determining the grain size distribution, it is necessary to measure the grain areas from a large number of equivalent simulations.

2.3 Histogram Analysis of Product Microstructures

2.3.1 Spatially Homogeneous Nucleation

In order to analyze the impact of heterogeneous nucleation on microstructure, it is first necessary to examine microstructures associated with homogeneous nucleation in some detail. While product grain size and shape are set by the areal nucleation site density and homogeneous nucleation rate in an infinite system, both small (lattice parameter) and large (system size) length cutoffs are inherent in simulations of nucleation and growth on a finite, periodic lattice and can affect the distribution of grain sizes. Thus, it is advantageous to understand just how these cutoffs influence microstructure in the absence of catalytic sites before proceeding to more complex cases.

Consider first the growth of product grains originating from a burst of nuclei which are distributed randomly throughout a two-dimensional system. The resulting microstructure consists of a collection of Voronoi grains which tile the system. The quantity of central importance in our microstructural analysis is the probability distribution, $P(A')$, of normalized grain areas, $A' = A/\bar{A}$, where $\bar{A}$ is the average area.[27] The histograms of the probability distributions for the condition of spatially random nucleation are shown in Fig. 2.1a for four different area densities n. As is

evident from the figure, these distributions can be described by a quasi-universal curve for relatively large values of n, as might be expected for a series of nearly self-similar structures. At somewhat smaller values of n, however, there is some small deviation in the histogram from its high-density counterparts. This shift can be understood in terms of the finite size of the system (in this case a 300 $\times$ 300 lattice) with the result that it is not possible to accurately sample large normalized grain areas A' at sufficiently small n or, equivalently, large $\bar{A}$. This will be shown explicitly below in a finite-size scaling analysis of the moments of $P(A')$. It should be pointed out here that no exact analytical form for $P(A')$ is known for this system. Gilbert, however, [24] has obtained the second moment of this distribution

$$\mu_2^A = 0.280\bar{A}^2, \tag{2.1}$$

and a number of other approximate results also exist. In particular, Kiang [28] has found that the gamma distribution fits the observed distribution of grain areas well, and Weaire et al. [29] have justified this result by using stereological arguments relevant to a Poisson point process in conjunction with some assumptions about (average) grain shape. In this case the standard gamma distribution [30]

$$P^\gamma(A') = \frac{1}{\beta^\alpha \Gamma(\alpha)} (A')^{\alpha-1} \exp(-A'), \tag{2.2}$$

where α and β are parameters, can be simplified by noting that, since the expectation value $\mathrm{E}(A') = 1$, $\alpha = 1/\beta$ and consequently the variance $\mathrm{Var}(A') = \beta$. Indeed, Fig. 2.1b shows the excellent fit between simulation data for a large value of n and P^γ for the choice $\beta = 1/\alpha = 0.274$.

As discussed above, the finite size of the simulation cell constrains the distribution of product grain sizes that can be sampled. At relatively high areal density n this constraint is not too severe as $\bar{A}$ is relatively small. [31] This can be seen

by examining the high-density histograms shown in Fig. 2.1a. If, however, n is relatively small, then it is of interest to study this dependence on system size more systematically. For this purpose it is convenient to examine the lower order moments of the distribution, as they embody the most significant information, and to employ a finite-size scaling analysis. The dependence of the second, μ_2, and third, μ_3, moments of the distribution (about the mean) on the inverse areal density $1/n$ is shown in Fig's. 2.2a and 2.2b, respectively, for several different site densities on a 300×300 lattice. From this analysis one finds via extrapolation that $\mu_2(n \to \infty) = 0.278 \pm 0.001$, in good agreement with the exact result. This finite-size study will be useful in the analysis of heterogeneous nucleation given below.

2.3.2 Spatially Heterogeneous Nucleation

Consider next the growth of product grains originating from nuclei which are located on a network of preferred sites in the system. As we wish to model nucleation on some underlying cell structure, the network is taken to be the set of available sites which comprise the boundaries of this structure. For simplicity we imagine the the underlying structure is also a collection of equiaxed Voronoi cells and that nucleation is restricted to locations on cell boundaries. Thus, the average underlying cell size, l_u, becomes an important new parameter in the characterization of the microstructure of product grains.

In the case of heterogeneous boundary nucleation it is expected that at least two length scales are required to characterize the system, one associated with the underlying grain size (l_u) and the other associated with the internuclear separation.

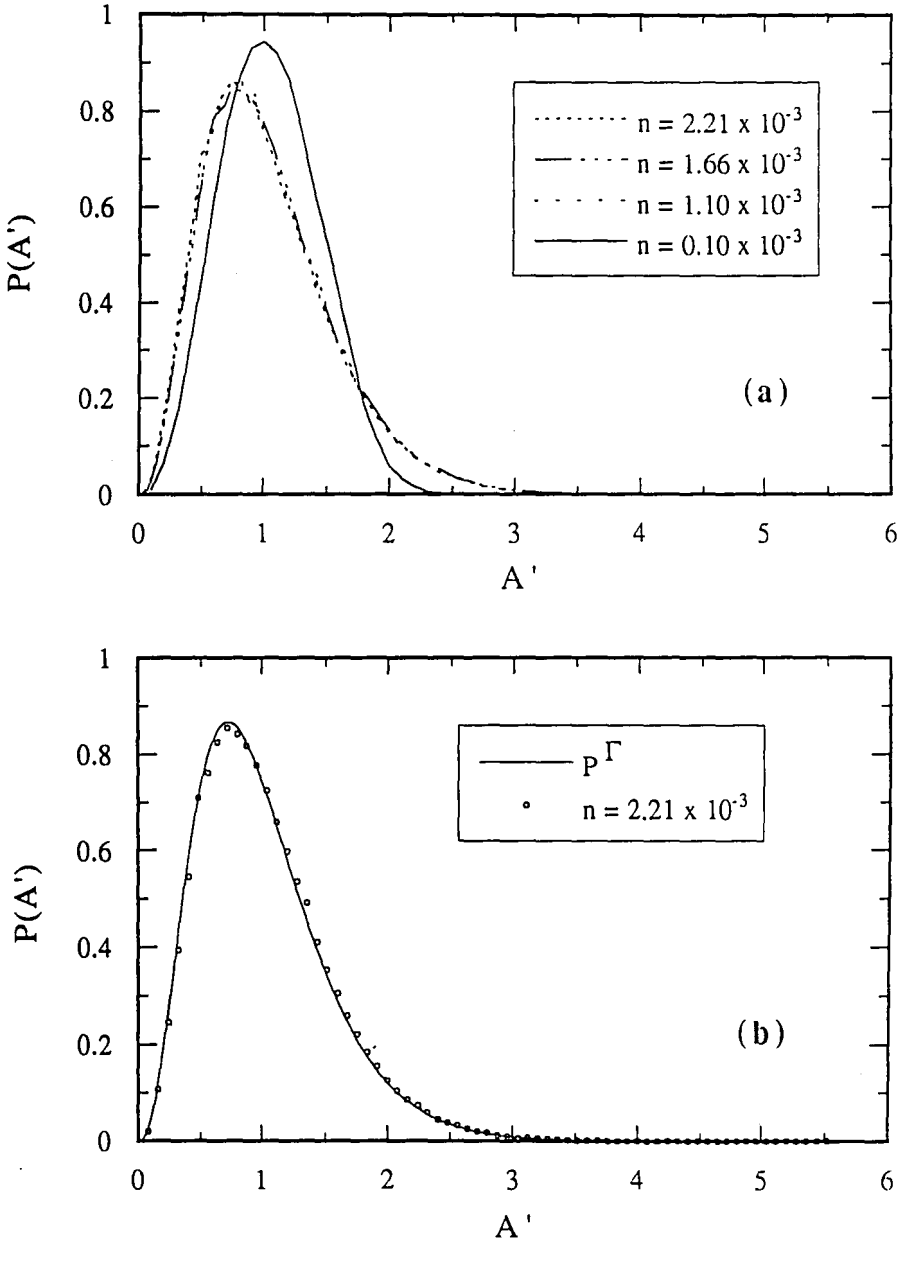

Figure 2.1: a.) The probability distributions $P(A')$ versus reduced area, $A' = A/\bar{A}$, for homogeneous nucleation in a two-dimensional system. The results for several different area densities, n, are shown. At relatively large values of n these histograms fall on a quasi-universal curve. At smaller values of n there is some deviation from this behavior. The histograms represent data for 7×10^4 to 1×10^6 grains. b.) The histograms corresponding to relatively large n given in the previous figure are fit to a gamma distribution (Eq. (2.2) with parameters $\beta = 1/\alpha = 0.274$. It should be noted that the fit is excellent. The histogram represents data for 1×10^6 grains.

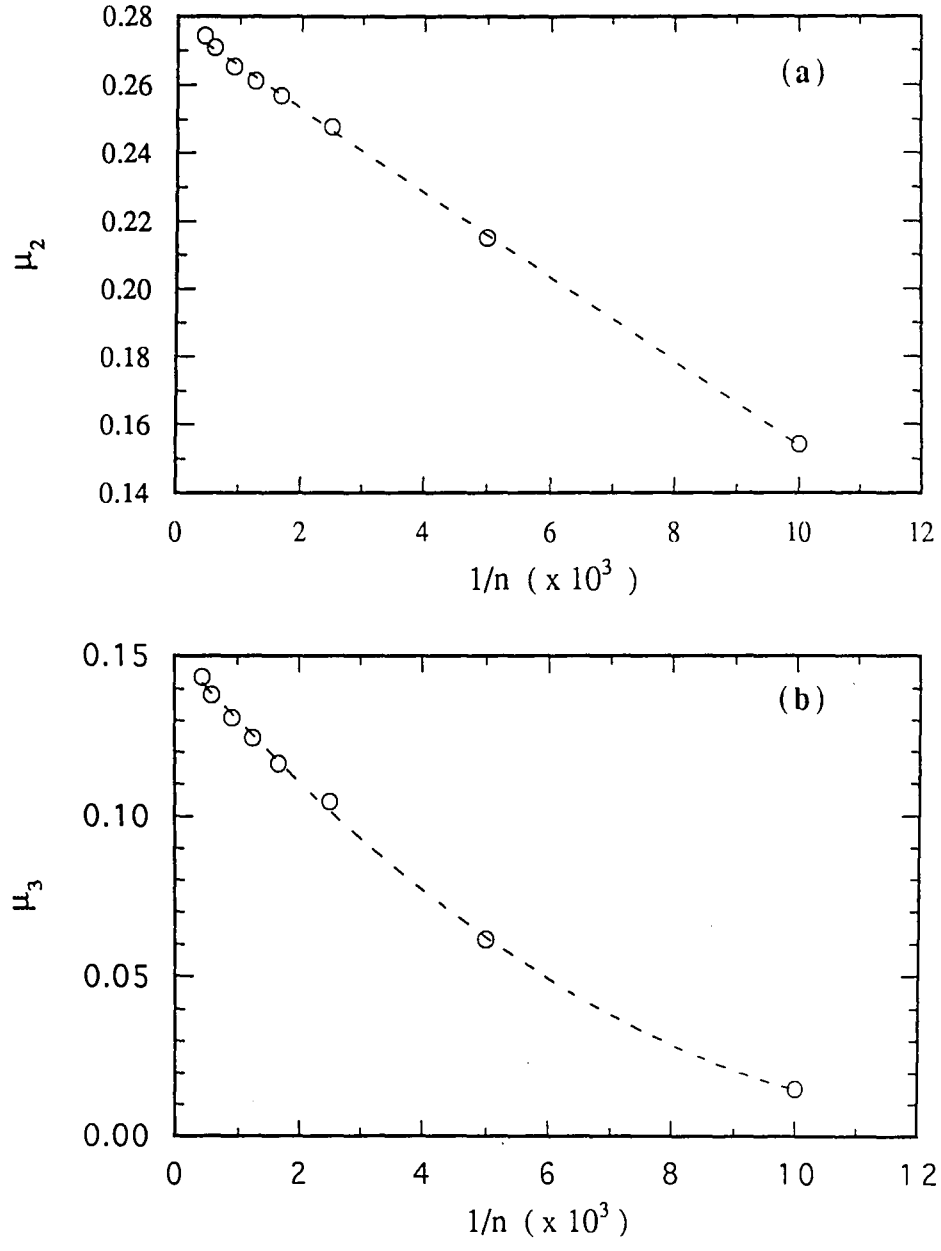

Figure 2.2: The dependence of the second, μ_2, (a) and the third, μ_3, moment (b) of the area distribution (about the mean) on the inverse areal density, $1/n$. This analysis permits the extrapolation of these moments to the infinite system limit. The dashed curves are linear and quadratic fits, respectively, in (a) and (b). In the case of the second moment $\mu_2(n \to \infty = 0.278)$

For the underlying structure $l_u = n_u^{-\frac{1}{2}}$, where n_u is the site density from which the underlying grain structure is generated. The average internuclear distance can be quantified in several ways. In this work we define the average separation along the boundary $l_b = \tilde{n}_b^{-1}$, where $\tilde{n}_b$ is the linear density of nuclei along the boundary network. That is, $\tilde{n}_b$ is the ratio of the number of nuclei to the number of available boundary sites. This is an approximation to the linear density which depends on lattice parameter. A more accurate estimate would naturally require a finer grid. It is, of course, also possible to base l_b on the areal nuclear density, though this is not an independent measure as stereological arguments can be used to relate the average underlying cell area to the average cell perimeter. For the subsequent discussion it is useful to define a relative measure of these length scales by the ratio

$$r = \frac{l_b}{l_u} \equiv \frac{\sqrt{n_u}}{\tilde{n}_b}. \tag{2.3}$$

Prior to the microstructural analysis, a number of intuitive conclusions can be inferred from this model. In the limit $r > 1$ one would predict that the product microstructure would be essentially equiaxed as the underlying structure should have little effect on widely separated nuclei. Conversely, in the limit $r < 1$, grains impinge first along the boundary and, in order to complete the transformation, must continue their growth in the direction normal to the boundary, thus creating elongated grains. The intermediate regime, corresponding to $r \sim 1$, is transitional in nature and will be investigated in some detail below.

These preliminary conclusions are borne out upon examining Fig.'s 2.3a-c which show the resultant microstructures for $log(r)$ = -0.781, -0.322 and 0.522 respectively.

It is clear that at large r the resultant microstructure becomes increasingly similar to that for homogeneous nucleation, namely a collection of nearly equiaxed

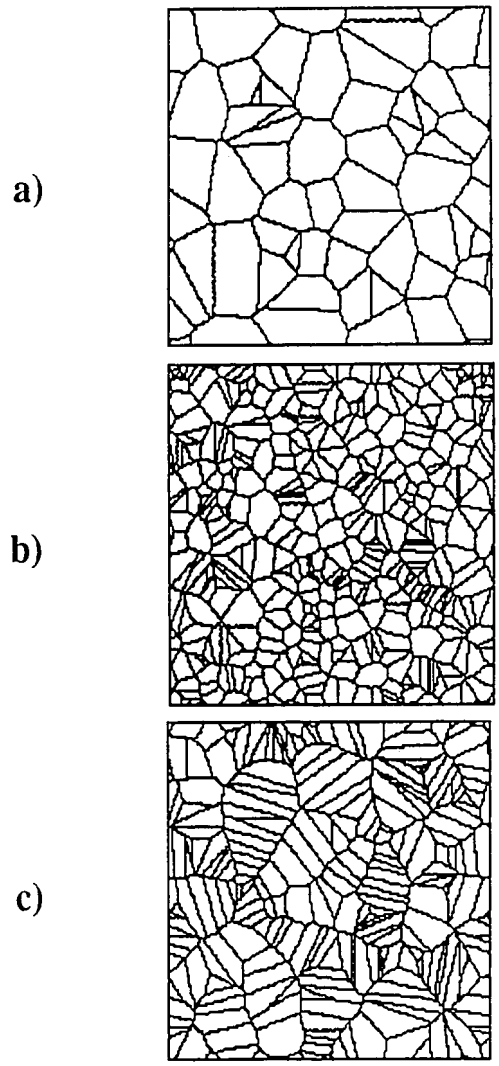

Figure 2.3: Several product grain microstructures for different values of the length ratio $log(r)$, namely -0.781(a), -0.322 (b) and 0.522(c). For relatively large r the product microstructure resembles that for homogeneous nucleation as it contains nearly equiaxed grains. At relatively small r many elongated grains are present.

grains. On the other hand, at small r, elongated grains with long axes normal to the boundary are dominant. The dependence of product grain area on r is summarized in Fig. 2.4a which shows the normalized grain size distribution for three different values of r.

It can be seen that with decreasing r the distribution shifts to the left, implying that a greater number of both relatively small and large grains is created. Again, there is a lower limit to the values of r which can be probed here due to the finite size of the lattice parameter. It is interesting to note that the gamma distribution describes $P(A')$ here as well. This is illustrated in Fig. 2.4b for a relatively high line density $\tilde{n}$. As in the case of homogeneous nucleation it is advantageous to examine the dependence of the moments of these probability distributions on the relevant length scales in the system.

Given that we wish to contrast heterogeneous with homogeneous nucleation, a natural quantity to calculate is the ith normalized moment for the heterogeneous system defined by

$$\mu_i^{norm} \equiv \frac{\mu_i}{\mu_i^{homo}(n)}, \tag{2.4}$$

where $\mu_i^{homo}(n)$ is the ith moment of the distribution for homogeneous nucleation and its dependence on the areal density n, as shown in Fig.'s 2.2, is emphasized. With this definition one can relate the variance, skewness, kurtosis, etc., of the grain area distribution to the corresponding quantities for a Voronoi grain area distribution that results from homogeneous nucleation and growth subsequent to a burst of nuclei with area density n.

Figure 2.5a is a common log-log plot of μ_2^{norm} versus r for a variety of underlying site densities n_u.

This normalized moment has been calculated using the same total number of

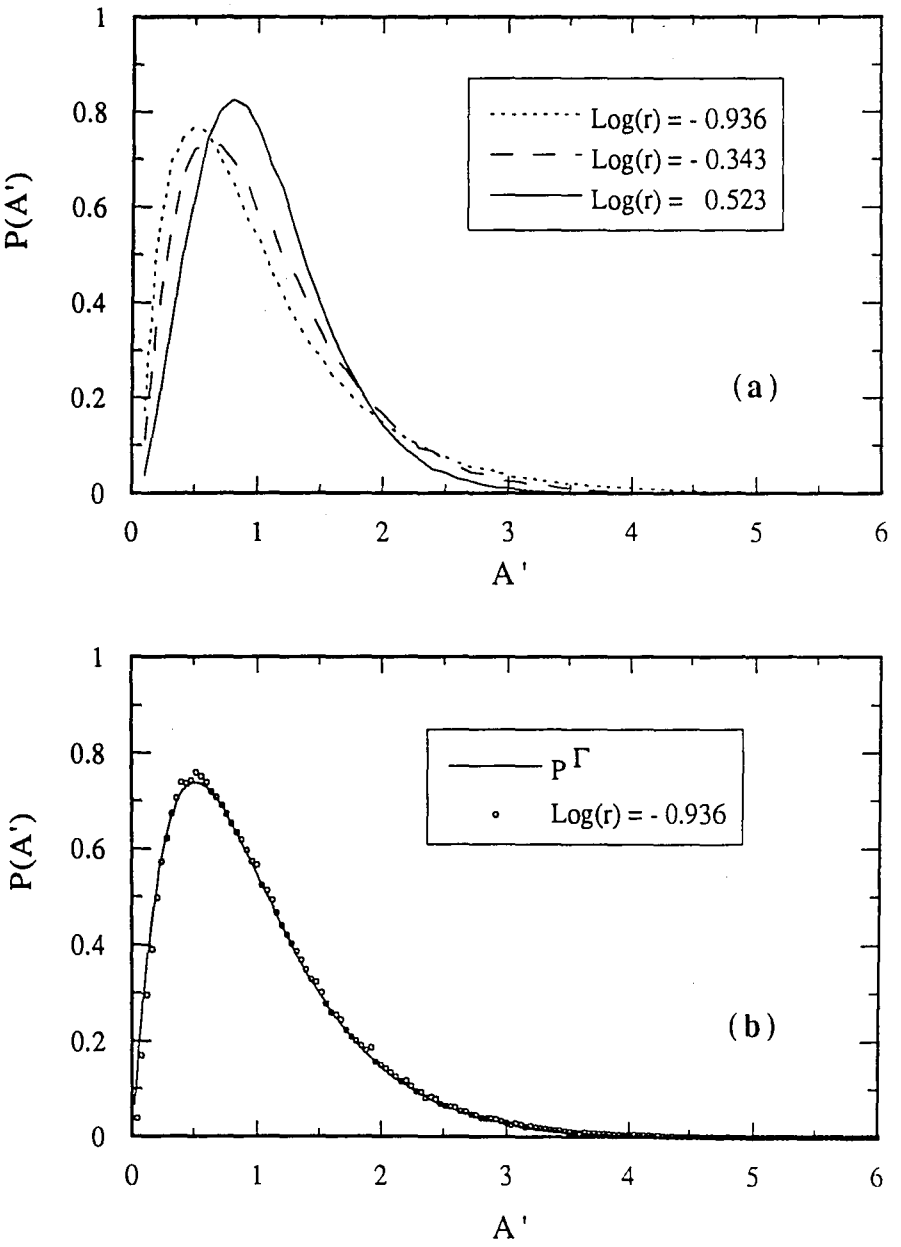

Figure 2.4: The probability distributions $P(A')$ versus reduced area, $A' = A/\bar{A}$, for heterogeneous nucleation in a two-dimensional system for various values of r. Note the shift of the histograms to the left upon decreasing r. The histograms represent data from 1×10^5 to 4×10^5 grains. b.) The probability distribution is fit to a gamma distribution with $\beta = 0.488$ for $log(r) = -0.520$.

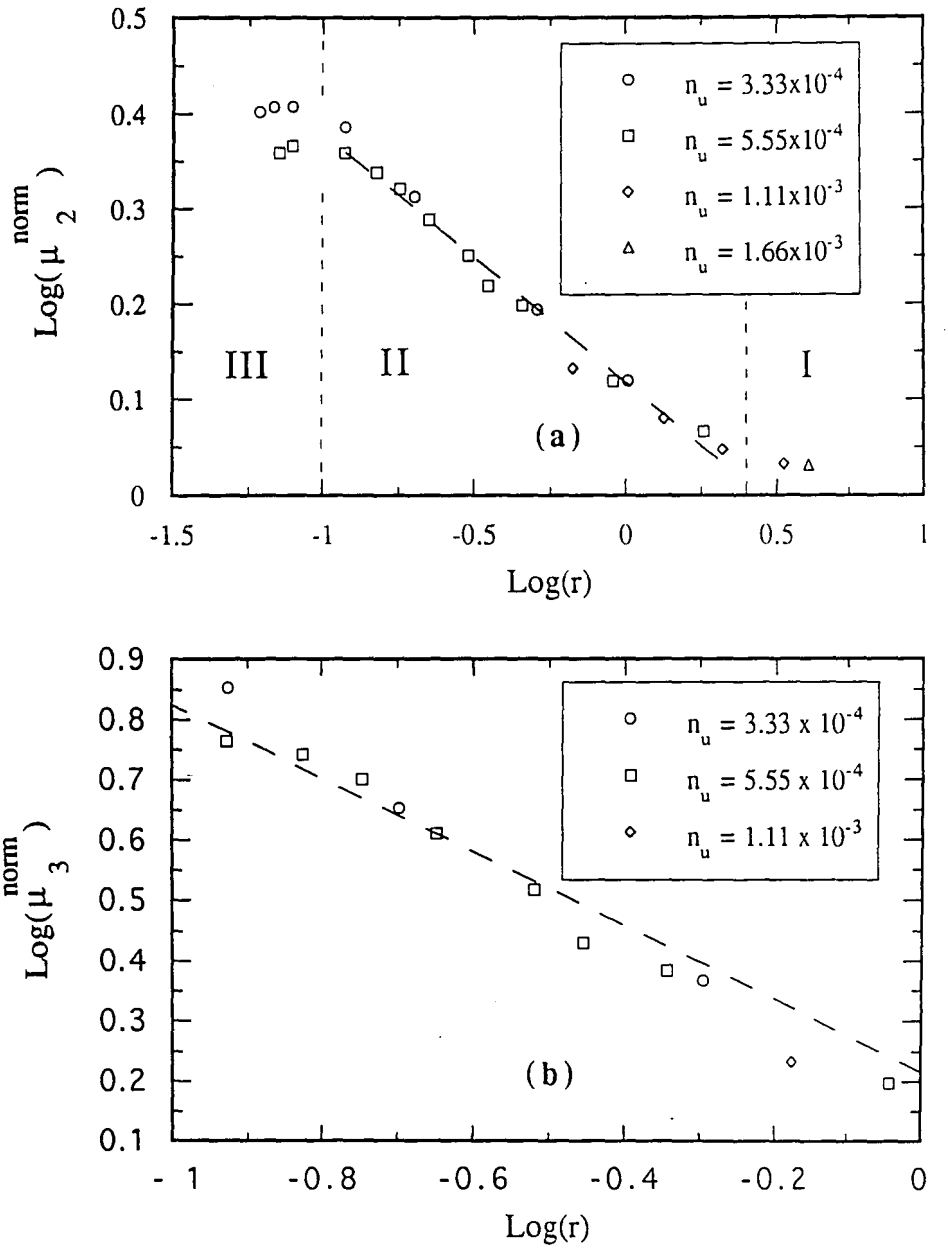

Figure 2.5: a.) The common log of the normalized second moment, μ_2^{norm}, versus the log of the length ratio, r, for heterogeneous nucleation for a variety of underlying site densities n_u. Three distinct regimes are identified in the text. b.) The common log of the normalized third moment, μ_3^{norm}, versus the log of the length ratio, r, for the same systems as in part a.

final grains in the system area for the two different nucleation conditions (heterogeneous vs. homogeneous) in order to mitigate the effects of system size on these moments. As is apparent from the figure, there exists three broad regimes of behavior. In regime I, where $\log(r) > 0$, the moments approach those for homogeneous nucleation and the associated microstructure is essentially equiaxed, as expected from the arguments above. In regime II, where $-1 < \log(r) < 0$, the spatial arrangement of neighbors about a given nucleus becomes somewhat anisotropic, and there is a concomitant change in the distribution of grain areas. It is tempting to describe this regime in terms of a power law, and this will be done for higher moments as well. In regime III, where $\log(r) < -1$, the moment ratio becomes much less sensitive to r for a given underlying structure. This can be understood by making the approximation that in this regime $P(A') \approx P_h(h')P_w(w')$, where P_h and P_w are probability densities for the normalized height and width, respectively, of the grains. That is, the distributions of grain heights and widths are taken to be nearly independent. Now, if it is further assumed that the distribution of nuclei along a cell boundary is describable as a Poisson process, then the grain widths should follow an exponential distribution with an average width given by $\tilde{n}_b^{-1}$. So, one finds that $\mu_2 \approx \mathrm{Var}(h')$, independent of the $\tilde{n}_b$. The behavior of the skewness of the distribution, as characterized by the normalized third moment μ_3, is shown in Fig. 2.5b for the important transitional regime, $-1 < \log(r) < 0$. Again, the data is well described by a power law in this regime.

Finally, it is possible to quantify the product grain elongation that attends high linear nucleation density, $\tilde{n}$, in the case of heterogeneous nucleation and growth. For the cell model of homogeneous nucleation and growth, it has been shown that the normalized perimeter, $\bar{P}/4\sqrt{\bar{A}} = 1$ [32]. In this work we found that $\bar{P}/4\sqrt{\bar{A}} =$

1.012 for a relatively small sample of 1000 grains. It is therefore expected that deviations from this result in the case of growth from a burst of nuclei located on a substructure will reveal associated deviations from equiaxedness. This can be seen by examining Fig. 2.6 which shows $\bar{P}/4\sqrt{\bar{A}}$ versus the parameter r for several different microstructures. occurred The increase in the normalized perimeter with decreasing r correlates with the prevalence of elongated grains seen in the microstructures (Fig.'s 2.3). For reference, at the high linear density given by $log(r)$ = -1.03 one finds that $\bar{P}/4\sqrt{\bar{A}} \approx 1.17$, which corresponds to (average) grain aspect ratios of between 3 and 4.

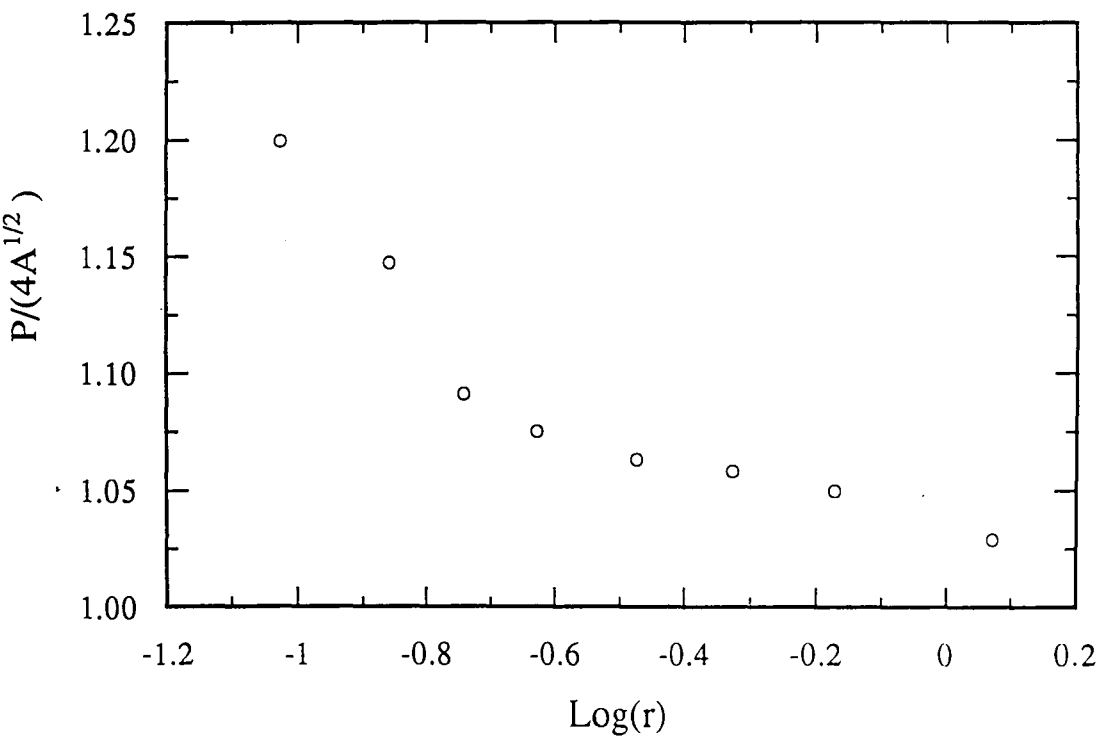

Figure 2.6: The normalized perimeter, versus length ratio, for a number of heterogeneous microstructures. The increase in the normalized perimeter with decreasing r correlates with grain elongation in the associated microstructures.

2.4 Discussion and Conclusions

In this work computer simulation has been employed in order to contrast the product grains size distributions resulting from spatially random and spatially biased nucleation. In both instances it was assumed that nucleation as a burst and subsequent grain growth proceeded at a constant radial growth rate until impingement. In the case of spatially biased nucleation, the nuclei were located on the boundaries between cells which define some underlying structure. For simplicity the underlying structure was modeled as a collection of Voronoi cells.

The influence of this underlying structure on the product microstructure was found to be well characterized, over a broad range of length scales, by the length ratio, r, (Eq. (2.3)) which relates the size of the underlying structure to the separation of product nuclei along boundaries. The area distributions associated with relatively large r displayed characteristics similar to those resulting from random nucleation, as seen from the behavior of their lower order moments. For the range $-1 < r < 0$, the moments obeyed an approximate power law relation and, in the corresponding microstructures, elongated grains were prevalent. The presence of non-equiaxed grains was quantified by calculating grain perimeter ratios for several microstructures and examining the dependence of this ratio on r.

One distinct advantage of simulation in studying the impact of nucleation conditions on product microstructure is that it permits a systematic variation of these conditions (i.e., underlying cell size, nucleation rate, etc.) in a "clean" system. The experimental reality is, of course, somewhat different, and the goal is to infer these nucleation conditions from an often limited amount of information. Indeed, the investigation of reactive phase formation in thin films, for example, utilizing a

variety of experimental techniques including differential scanning calorimetry and electron microscopy has shed some light on the nucleation and growth process in these systems and has been an active research area [14] [33]. Nevertheless, it has proven difficult to uniquely deduce such important parameters as the number and distribution of catalytic sites from experiments. In this regard, a more detailed microstructural analysis may be helpful. As shown in this paper, the moments of grain area distributions contain valuable information on relevant length scales in the system and therefore reflect the presence of preferential nucleation sites. By combining this analysis with measurements of area fraction transformed and the dynamic structure factor [25], it should be possible to get a better handle on the role of catalytic sites in a phase transformation. Further, detailed simulation studies are useful guides for experimentalists as they identify relevant parameters in the problem.

Bibliography

[1] J.W. Mayer and S.S Lau. *Electronic Materials Science: For Intergrated Circuits in Si and GaAs.* Macmillan Publishing Company, New York, 1990.

[2] J.D. Gunton and M. Droz. *Introduction to the Theory of Metastable and Unstable States.* Springer, Berlin, 1983.

[3] For a recent review of the decay of metastable states see P. A. Rikvold and B. M. Gorman in *Annual Reviews of Computational Physics I* ed. by D. Stauffer World Scientific, Singapore, (1995), p. 149.

[4] A.N. Kolmogorov. *Bull. Acad. Sci. USSR, Phys. Ser.*, 1(355), 1937.

[5] M. Avrami. *J. Chem. Phys.*, 7:1103, 1939. See also W.A. Johnson and R.F. Mehl, Trans. AIME **135**:416, 1939.

[6] K. Sekimoto. *Physica*, 135A:1356, 1986.

[7] G. Yu and J.K. Lai. *J. Appl. Phys.*, 79:3504, 1996.

[8] J.W. Cahn. *Acta. Metall.*, 4:572, 1956.

[9] L.A. Clevenger, C.V. Thompson, R.R. de Avillez, and E. Ma. *J. Vac. Sci. Technol. A*, 69:1566, 1990.

[10] L. A. Clevenger and C. V. Thompson. *J. Appl. Phys.*, 3:1325, 1990.

[11] E.G. Colgan. *Mater. Sci. Rep.*, 5, 1990. and references therein.

[12] B.M. Clemens and R. Sinclair. *MRS Bulletin*, XV(2):19, 1990.

[13] K.R. Coffey, K. Barmak, D.A. Rudman, and S. Foner. *J. Appl. Phys.*, 72:1341, 1992.

[14] K. R. Coffey, L. A. Clevenger, K. Barmak, D. A. Rudman, and C.V. Thompson. *Appl. Phys. Lett.*, 55:852, 1989.

[15] K. Barmak, K.R. Coffey, D.A. Rudman, and S. Foner. *J. Appl. Phys.*, 67:7313, 1990.

[16] A.S. Edelstein, R.K. Everett, G.Y. Richardson, S.B. Qadri E.I. Altman, J.C. Foley, and J.H. Perepezko. *J. Appl. Phys.*, 76:7850, 1994.

[17] E. Ma, C.V. Thompson, and L.A. Clevenger. *J. Appl. Phys.*, 4:2211, 1991.

[18] K. Barmak, C. Michaelsen, and G. Lucadamo. *J. Mater. Res.* submitted for publication.

[19] C. Michaelsen, S. Wöhlert, R. Bormann, and K. Barmak. *Mat. Res. Soc. Symp. Proc.* in Press.

[20] K. Barmak, S. Vivekanand, F. Ma, and C. Michaelsen. *Mat. Res. Soc. Symp. Proc.* in Press.

[21] K. Mahin, K. Hanson, and J.W. Morris Jr. *Acta. Metall.*, 28:443, 1980.

[22] H.J. Frost and C.V. Thompson. *Acta. Metall.*, 35:529, 1987.

[23] Q.Z. Hong, K. Barmak, and L.A. Clevenger. *J. Appl. Phys.*, 72:3423, 1992.

[24] E.N. Gilbert. *Ann. Math. Stat.*, 33:958, 1962.

[25] J.M. Rickman, W.S. Tong, and K. Barmak. to be published in Acta Metall. Mater.

[26] D. Weaire and J. Wejchert. Computer models of froths and voronoi patterns. In D.J. Srolovitz, editor, *Computer Simulations of Microstructural Evolution*, Warrendale, PA, 1986. The Metallurgical Society.

[27] For consistancy, throughout the paper we will denote a quantity normalized by its average with a prime.

[28] T. Kiang. *Z. Astrophys.*, 48:433, 1966.

[29] D. Weaire, J.P. Kermode, and J. Wejchert. *Phil. Mag. B*, 53:L101, 1986.

[30] J.E. Freund and R.E. Wadpole. *Mathematical Statistics.* Prentice Hall, Englewood Cliffs, NJ, 1980.

[31] Clearly there is an upper limit to the density n which can be studied. If $\sqrt{1/n}$ is of the order of the lattice parameter, then it will not be possible to accurately sample relatively small grains.

[32] J.L. Meijering. *Phillip. Res. Rep.*, 8:270, 1953.

[33] K. Barmak, C. Michaelsen, J. Rickman, and M. Dahms. *Mat. Res. Soc. Symp. Proc.* in press.

Appendix A

Correlation Functions

In this Appendix the calculation of nonequilibrium, two-point functions is briefly summarized. Consider first the case of spatially random nucleation which occurs as a burst near the origin of time. From Eq. (1.2) one can construct the equal-time, two-point funct ion

$$C_2(\vec{r}_1,\vec{r}_2,t) = \exp\left[-n\int d^2r'\,(1 - D(\vec{r}_1;t:\vec{r}';0)D(\vec{r}_2;t:\vec{r}';0))\right] \qquad \text{(A.1)}$$

corresponding to the nucleation rate given in Eq. (1.4) and interface-controlled growth kinetics. This equation can be rewritten upon inserting the appropriate expressions for the D functions as

$$C_2(\vec{r}_1,\vec{r}_2,t) = [C_1(t)]^2 \exp[n\int d^2r'\Theta(Gt - |\vec{r}_1 - \vec{r}'|)\Theta(Gt - |\vec{r}_2 - \vec{r}'|) \qquad \text{(A.2)}$$

and then transformed by a change of variable to

$$C_2(\vec{r}_1,\vec{r}_2,t) = [C_1(t)]^2 \exp[n\int d^2u\Theta(Gt - |\vec{u}|)\Theta(Gt - |\vec{u} + \vec{\delta}|), \qquad \text{(A.3)}$$

where $\delta \equiv \vec{r}_1 - \vec{r}_2$.

Now, the integral in the exponential can be performed by noting its geometrical interpretation, as shown in Fig. A.1. As the grains are circular the orientation of δ is immaterial. The value of the integral is given by the area of overlap in the figure. One method to calculate this area is to fill the shaded region with a series of strips of infinitesimal width and then integrate over the width. By using this approach one obtains (Eq. (1.7))

$$C_2(\delta, t) = [C_1]^2 \exp(n\pi G^2 t^2 \gamma(s)), \tag{A.4}$$

where

$$\gamma(s) = \frac{2}{\pi} \left[sin^{-1}\sqrt{1-s^2} - s\sqrt{1-s^2} \right] \Theta(1-s). \tag{A.5}$$

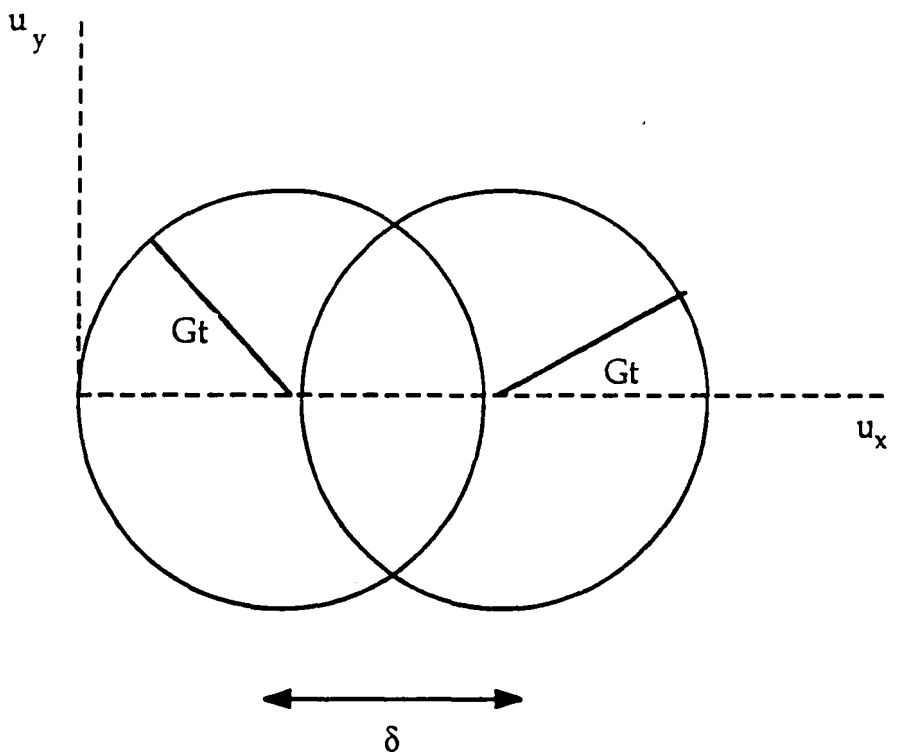

Figure A.1: A geometrical picture of the integration to be performed in Eq. (A3). The required integral is the area of overlap of the two circles shown here.

Vita

William Scott Tong was born to Wyman and Bonita Tong on November 2, 1971 in Honolulu, Hawaii. After realizing his preference to math and science while attending Punahou Schools, he traveled to Lehigh University to study engineering, where he graduated with a B.S. in Materials Science and Engineering.

In his spare time, he enjoys reading, playing basketball, and comunicating with friends. In the future he expects to continue his education, although the specific institution is not known at this time.

END

OF

TITLE